# Petrogenesis of the Mesozoic Shuikoushan peraluminous I-type granodioritic intrusion in Hunan Province, South China: Middle–lower crustal reworking in an extensional tectonic setting

Jie-Hua Yang [a,b,*], Jian-Tang Peng [a,c], Yong-Fei Zheng [b], Rui-Zhong Hu [a], Xian-Wu Bi [a], Jun-Hong Zhao [d], Jin-Chuan Huang [a], Bang-Lu Zhang [a]

[a] State Key Laboratory of Ore Deposit Geochemistry, Institute of Geochemistry, Chinese Academy of Sciences, Guiyang 550002, China
[b] School of Earth and Space Sciences, University of Science and Technology of China, Hefei 230026, China
[c] School of Geosciences and Info-physics, Central South University, Changsha 410083, China
[d] State Key Laboratory of Geological Processes and Mineral Resources, China University of Geosciences, Wuhan 430074, China

### A B S T R A C T

The Mesozoic Shuikoushan granitoid intrusion in the Jiangnan orogen between the Yangtze and the Cathaysia blocks in southern Hunan Province, South China, provides an opportunity to probe deep-crustal composition and structure, and to investigate the geodynamic evolution of South China. The intrusion is composed of granodiorite with I-type geochemical affinities and contains zircon with an U–Pb concordant age of $158.3 \pm 1.2$ Ma. Rocks from the intrusion have variable $SiO_2$ from 58.4 wt.% to 65.2 wt.%, $Al_2O_3$ from 15.0 wt.% to 17.2 wt.%, $TiO_2$ from 0.57 wt.% to 0.76 wt.%, and $P_2O_5$ from 0.27 wt.% to 0.52 wt.%. They have A/CNK from 0.97 to 1.23 (1.04 on average) and are dominantly peraluminous. They are characterized by enrichment in LREE ($[La/Sm]_N = 3.47$–5.19) and LIL (e.g., K, Rb) and depletion in HFSE (e.g., U, Th) in primitive mantle normalized trace element diagrams. These geochemical features indicate that the rocks are I-type granodiorites and have undergone extensive fractional crystallization of hornblende, biotite, titanite, and apatite. All samples show negative $\varepsilon_{Hf}(t)$ (−10.6 to −8.1) and $\varepsilon_{Nd}(t)$ (−5.92 to −6.13) values, with relatively high initial $^{87}Sr/^{86}Sr$ ($I_{Sr}$) (0.7101–0.7102) and $\delta^{18}O$ ratios (8.4–9.7‰). These values significantly differ from mantle values, suggesting that they are generated by the amphibole-dehydration melting of a mafic source in the middle-to-lower crust beneath the Jiangnan orogen. The emplacement of the Shuikoushan granitoid intrusion is contemporaneous with the late Jurassic to early Cretaceous extension within the Shi-Hang rift zone, indicating that it may have been formed under an extensional regime in response to both the Pacific superplume activity and westward subduction of the Pacific Plate. The extensional processes along with asthenosphere upwelling and basaltic underplating may have triggered the widespread late Jurassic granitoid intrusion in southern Hunan Province and possibly in South China.

© 2016 Elsevier Ltd. All rights reserved.

## 1. Introduction

Peraluminous granitoids usually have aluminum saturation index [ASI = molar $Al_2O_3/(CaO + Na_2O + K_2O)$] higher than 1.0 (Zen, 1986). They are widely spread in orogenic belts (e.g., the Himalayan and Jiangnan orogenic Belt in China) and certain types of subduction-related environments (e.g., the Nevada batholith in USA) (Barbarin, 1996; Sylvester, 1998; Lackey et al., 2006; Chappell et al., 2012; Zhao et al., 2013; Chen et al., 2014). Recent studies reveal that these granitoids can also be formed in extensional tectonic settings (Turpin et al., 1990; Sun et al., 2005). Despite numerous studies, their origins and petrogenesis have long been matters of debate and remain obscure to most geologists, but are very important in evaluating crustal growth/reworking, and addressing thermal and geodynamic evolution (Patiño Douce and Johnston, 1991; Barbarin, 1996; Sylvester, 1998; Castro et al., 1999; Clemens et al., 2011; Chappell et al., 2012; Zhao et al., 2013; Chen et al., 2014).

It is generally accepted that peraluminous granitoids are mainly composed of S-type rocks. These rocks are assumed to be derived from the partial melting of supracrustal metasedimentary rocks and are characterized by the enrichment of aluminum (Al) and

* Corresponding author at: State Key Laboratory of Ore Deposit Geochemistry, Institute of Geochemistry, Chinese Academy of Sciences, Guiyang 550002, China.
    *E-mail address:* yangjiehua@mail.gyig.ac.cn (J.-H. Yang).

potassium (K) (Chappell, 1999; Chappell and White, 1974, 1992, 2001; Chappell et al., 2012). However, many I-type granitoids are also peraluminous and K-rich, despite having metaluminous source and not being saturated in Al and K. It remains unclear how peraluminous I-type granitoids were generated from such materials. Some models for peraluminous I-type granitoid rock formations have been proposed, such as the partial melting of K-rich meta-andesites (Roberts and Clemens, 1993); reactive assimilation of metapelites by high-alumina basaltic magmas (Patiño Douce, 1995); simple mixing of felsic, metasediment-derived, and basaltic magmas (Davis and Hawkesworth, 1993); the melting of more mafic source rocks, accompanied by assimilation of sedimentary rocks (Ugidos and Recio, 1993; Chappell et al., 2012); and fractional crystallization (Cawthorn and Brown, 1976; Zen, 1988; Schaltegger and Corfu, 1992).

The Shuikoushan peraluminous I-type granitoids are located in southern Hunan Province, between the Yangtze and the Cathaysia blocks, South China. Taking its special tectonic location and geochemical characteristics into consideration, there has long been an argument regarding their petrogenesis and geodynamic setting. For example, some studies argued that the Shuikoushan granitoids likely represent recycled crustal materials within the Cathaysia Block during the late Jurassic, without crustal growth (Zuo et al., 2014). By contrast, other studies concluded that the Shuikoushan granitoids were derived from depleted mantle with minor crustal contamination, as well as abundant crustal growth in the Yangtze Block during the early Jurassic period (Wang et al., 2002, 2003a,b; Ma et al., 2006). Whole-rock compositions provide only cumulative evidence for the complex processes that ultimately determine magma compositions. However, robust accessory minerals such as zircon, which preserves chemical evidence for stable and radiogenic isotope compositions of their host magmas at the time of crystallization, can be *in situ* analyzed to reveal different magmatic processes at high temporal and spatial resolutions (Li et al., 2014). Improvements in the micro-analysis of accessory minerals now allow high-precision, high-spatial resolution *in situ* analyses of zircon isotope compositions to be integrated with U–Pb dating to reveal a detailed record of magma sources and their evolution (Valley et al., 2005; Kemp et al., 2007; Li et al., 2010a, 2014).

In this study, high-precision and high-spatial resolution microanalytical isotope techniques were applied to determine the chronology and test the synchronicity of the Shuikoushan granitoid intrusion relative to regional and tectonic evolution. Within this framework, *in situ* zircon Hf and O isotopes and whole-rock geochemistry were used to identify the special magmatic source and process for granitoids from Shuikoushan intrusion. These new findings were used to examine the interrelated magmatic and tectonic processes that have caused the distinguishing characteristics of the Shuikoushan granitoids relative to other granitoids in its adjacent region.

## 2. Geological background, samples, and petrography

South China consists of the Yangtze Block in northwest and the Cathaysia Block in the southeast. These two blocks are commonly considered to have welded together along the Jiangshan–Shaoxing Fault (Jiangnan Orogenic Belt) in the middle Neoproterozoic period (Fig. 1) (Chen and Jahn, 1998; Zhao et al., 2011; Zhao, 2015; Yao et al., 2015). The Yangtze Block is composed of minor Archean–Paleoproterozoic crystalline basement rocks that are outcropped near the Yangtze Gorge Dam, including TTG (tonalite, trondhjemite, and granodiorite) gneisses, metasedimentary rocks, and amphibolites (e.g., the Kongling complex in Hubei Province) (Chen and Jahn, 1998; Wang et al., 2006; Jiao et al., 2009; Zhang and Zheng, 2013; Zhao and Asimow, 2014). Variably deformed,

low- to medium-grade metamorphic rocks of late Mesoproterozoic to early Neoproterozoic are sporadically distributed around the periphery of the Yangtze Block (Zhang and Zheng, 2013). The magmatic rocks are unconformably overlain by weakly metamorphosed Neoproterozoic strata (e.g., Banxi Group) and unmetamorphosed Sinian cover (Zheng et al., 2013). Unlike the Yangtze Block that contains the Archean basement, the Cathaysia Block is composed predominantly of Neoproterozoic basement rocks with a minor occurrence of Paleoproterozoic rocks in the southwest Zhejiang and north Fujian Provinces, and Mesoproterozoic rocks in Hainan Island (Zheng et al., 2013; Zhao and Asimow, 2014). Both basement blocks are overlain by Paleozoic continental to neritic marine sediments as well as continental redbeds and volcanicsedimentary sequences from the late Triassic time onward. The entire sequence is intruded by voluminous granitoid pluton (Chen and Jahn, 1998; Wang et al., 2003b; Yan et al., 2003; Qiu et al., 2016). However, the position of the subsurface boundary between the Yangtze Block and Cathaysia Block has been debated because of multiperiod tectonic interference. Previous studies have roughly defined the position of the suture zone between the Yangtze and the Cathaysia blocks (Chen et al., 1991; Rao et al., 2012) (Fig. 1). Mesozoic volcanic and intrusive rocks are widely exposed in the suture zone in Hunan Province (Fig. 1), some of which are closely associated with large to giant Cu–Pb–Zn multimetal deposits (e.g., the Baoshan granitoid, Tongshanling granitoid, and Shuikoushan granitoid) (Fig. 2a).

The Shuikoushan granitoid intrusion is located in this suture zone between the Yangtze and the Cathaysia blocks, and to the north of the NE-trending Jurassic Shi-Hang rift zone (Fig. 1). This intrusion is associated with Cu–Pb–Zn deposits, as well as gold and magnetite ore mineralization (Huang et al., 2015) (Fig. 2b). The other granitoid intrusions (e.g., Tongshanling and Baoshan) in the region only host Cu–Pb–Zn deposits. The Shuikoushan intrusion occurs as a lopolith with outcrop of 1.2 km wide and 1.6 km long, and intruded into the Carboniferous and Permian sedimentary sequence that consist of limestone and Carboniferous (Fig. 2b). The studied samples were collected from the adits of the Laoyachao mining in Shuikoushan area, and away from ore lodes. All samples were relatively fresh, free of weathering and alteration. They are predominantly granitoids that consist of plagioclase (35–40%), alkali feldspar (10–15%), quartz (10–20%), biotite (5–10%), hornblende (5–8%), and minor amounts of sphene, apatite, zircon, Fe–Ti oxides, and allanite (Fig. 3). These granitoids are mediate grain and show subhedral granular textures. Some samples, however, show porphyritic textures. The phenocrysts are commonly plagioclase, quartz, biotite, and hornblende; and the matrix is mainly composed of fine-grained feldspar and quartz with minor biotite, hornblende, and opaque oxides. Euhedral to subhedral plagioclase phenocrysts are 2–4 mm long and display optical zonation. Hornblende shows brown to green polychroism (Fig. 3). In general, Shuikoushan granitoids have a higher proportion of biotite and hornblende but less alkali feldspar and quartz as compared with the other granitoids in the region.

## 3. Analytical methods

### 3.1. SIMS zircon U–Pb dating and in-suit O isotope analyses

Zircon concentrates were separated from ca. 2-kg of rock samples using conventional heavy liquid and magnetic separation techniques at the mineral separation laboratory of the Bureau of Geology and Mineral Resources of Hebei Province at Langfang city. Representative zircon grains were handpicked under a binocular microscope. Zircon grains were mounted in epoxy mounts, which was then polished to section the crystals in half for analysis.
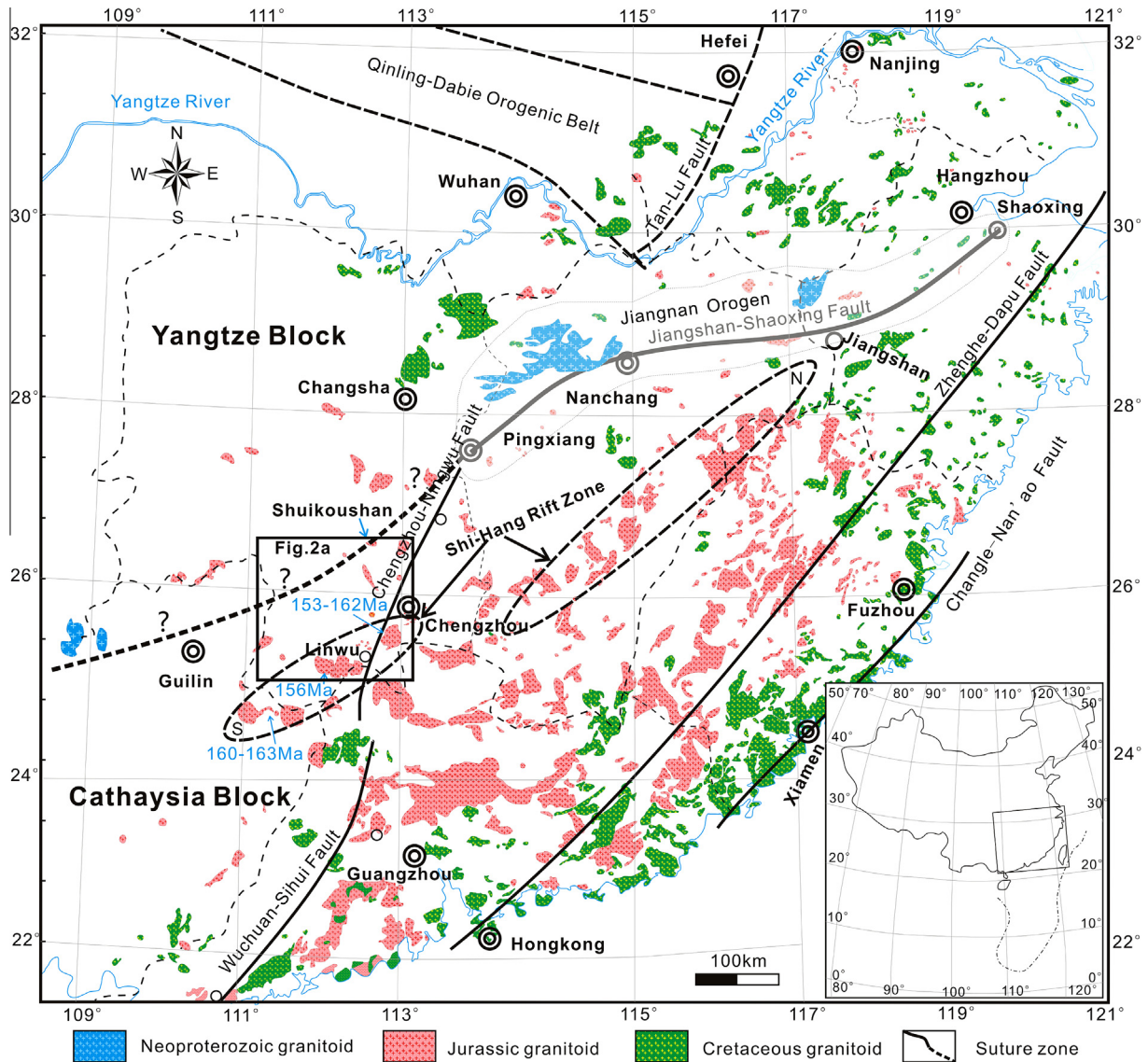
**Fig. 1.** Geological sketch map of South China modified from Chen and Jahn (1998), Sun (2006), Zhu et al. (2006), and Rao et al. (2012), showing distribution of Jurassic, Cretaceous and Neoproterozoic granitoid. The Shuikoushan granitoid intrusion is located in the suture zone between the Yangtze and the Cathaysia blocks, to the north of Shi-Hang rift zone (N: the north belt, S: the south belt). Isotopic dating Shi-Hang belt A-type granites from Zhu et al. (2008).

All zircons were documented with transmitted and reflected light micrographs as well as cathodoluminescence (CL) images to reveal their internal structures, and the mount was vacuum-coated with high-purity gold film prior to SIMS analyses.

U–Pb dating was carried out following oxygen isotope analysis using a Cameca IMS 1280 SIMS at the Institute of Geology and Geophysics, Chinese Academy of Sciences in Beijing. Analytical procedures are the same as those described by Li et al. (2009b). A ca. 8 nA primary $O^{2-}$ beam was used for zircon analysis with 13 kV impact energy. The analytical pits were about $20 \times 30\ \mu m$ in size and ellipsoidal in shape. Positive secondary ions were extracted with a 10 kV potential. Pb ion yields were increased by a factor of ~2 by flooding the sample surface with oxygen. In the secondary ion optics, a 60 kV energy window was used, together with a mass resolution of ca. 5400, to separate Pb ion peaks from isobaric interferences. The field aperture was set to 7000 μm, and the transfer optic magnification was adjusted to 200. Rectangular lenses were activated in the secondary ion optics to increase the transmission at high mass resolution. A single electron multiplier was used in ion-counting mode to measure secondary ion beam

intensities by peak jumping. Each measurement consists of 7 cycles, and the total analytical time is ca. 14 s. Pb/U calibration was performed relative to standard zircon 91500 with U and Th concentrations of ca. 81 and 29 ppm, respectively (Wiedenbeck et al., 1995). Analyses of the standard zircon Plésovice were carried out after every 3–4 unknown analyses. U–Th–Pb rations were calibrated against measured rations of standard zircon Plésovice with an age of 337 Ma (Sláma et al., 2008). A long-term uncertainty of 1.5% (1SD) for $^{206}Pb/^{238}U$ measurements of the standard zircons and the error of the unknown analysis were propagated to the unknowns. Measured composition were corrected for common Pb using non-radiogenic $^{204}Pb$. Corrections are sufficiently small to be insensitive to the choice of common Pb composition, and an average of present-day crustal composition (Stacey and Kramers, 1975) is used for the common Pb assuming that the common Pb is largely surface contamination introduced during sample preparation. Data reduction was carried out using the Isoplot/Ex v. 4.15 programs (Ludwig, 2008).

In order to monitor the external uncertainties of SIMS U–Pb measurements calibrated against Plésovice standard, Qinghu
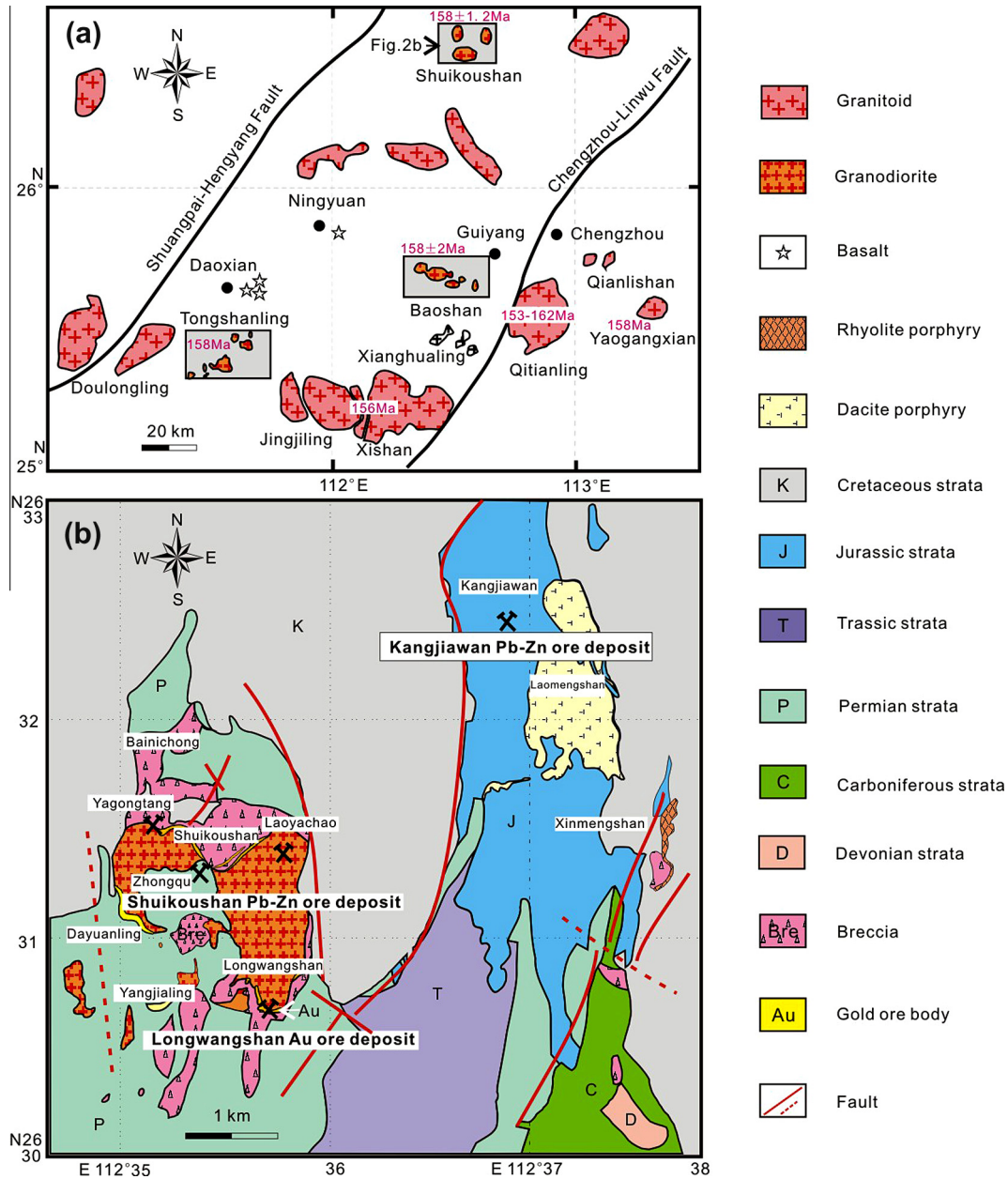
**Fig. 2.** Geological sketch map of the Shuikoushan mining district and adjacent region. (a) Simplified geological map of the southern Hunan Province modified from Wang et al. (2002) and Zhao et al. (2012), showing the distribution of diorite–granodiorite. Isotopic dating from Lu et al. (2006) and Zhu et al. (2008), and this study. (b) Geological map of the Shuikoushan mining district modified from Zuo et al. (2014).

zircon standard was alternately analyzed as an unknown together with the unknown zircons. A total of 5 measurements were onducted on Qinghu zircon, and the Concordia Age of 161.2 ± 2.3 Ma (2SD), which is identical within error with the recommended value of 159.2 ± 0.2 Ma (2SD) (Li et al., 2013).

Zircon oxygen isotopes were also measured using the Cameca IMS 1280 SIMS at the Institute of Geology and Geophysics following the methods described by Li et al. (2010a), with data reported as per mil (‰) value relative to Vienna Standard Mean Ocean Water (VSMOW, $^{18}O/^{16}O$ = 0.0020052). A primary $Cs^+$ ion beam of about 20 μm diameter was accelerated at 10 kV, and used at intensity of ca. 2 nA. The normal incidence electron flood gun was used compensate for sample charging during analysis with homogeneous electron density over a 100 μm oval area. Negative secondary ions were extracted with a −10 kV potential. Oxygen isotopes were measured using multi-collection mode. The mass

resolution used to measure of 20 cycles, each lasting 3 s, with an internal precision better than 0.2‰ (1σ). The instrumental mass fractionation (IMF) is calibrated against the Penglai zircon standard ($δ^{18}O$ = 5.31 ± 0.10‰) (Li et al., 2010b). In order to monitor the external uncertainties of SIMS O measurements calibrated against Penglai standard, Qinghu zircon standard was alternately analyzed as an unknown together with the unknown zircons. Six measurements of the Qinghu zircon standard during the course of this study yield a weighted mean of $δ^{18}O$ = 5.41 ± 0.15‰ (2SD), which is consistent within error the reported value of $δ^{18}O$ = 5.4 ± 0.2‰ (2SD) (Li et al., 2013).

### 3.2. LA-MC-ICPMS Lu–Hf isotope analyses

Zircon Hf isotope analysis was carried out on a Neptune multi-collector ICPMS equipped with Geolas-2005 excimer Arf
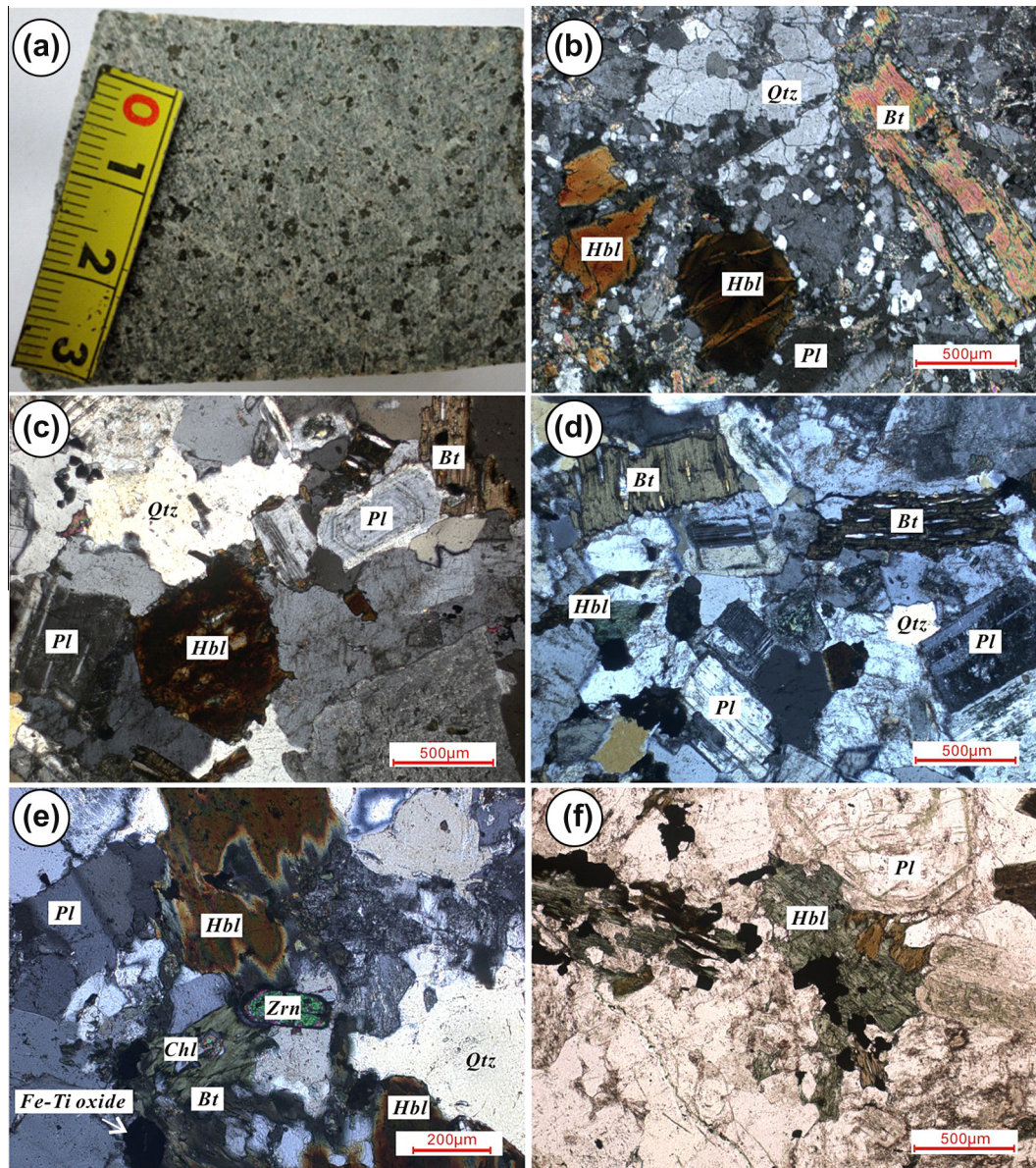
**Fig. 3.** Petrographic characteristics of Shuikoushan granodiorites: the characteristic of hand specimen of Shuikoushan granodiorites; photomicrograph of the Shuikoushan granodiorite consisting of quartz, plagioclase, biotite, and hornblende (b–f). Images (b), (c), (d), and (e) are in cross-polarized light (CPL), and image (f) is in plane-polarized light (PPL). Abbreviations: Qtz: quartz; Pl: Plagioclase; Bt: Biotite; Hbl: Horndlende; Zrn: Zircon; Chl: Chlorite.

laser ablation system (LA-MC-ICPMS) at the State Key Laboratory of Geological Processes and Mineral Resources, China University of Geosciences (Wuhan). Lu–Hf isotopic measurements were made on similar sites of the same zircon grains previously analyzed for U–Pb and O isotopes, with ablation pit of 44 μm in diameter. Each measurement comprised 3 s acquisition of the background signal followed by 50 s signal acquisition. The detailed analytical procedures were similar to those described by Hu et al. (2012). Off-line selection and integration of analytic signal, and mass bias calibrations were performed using ICPMSDateCal (Liu et al., 2010). The value $^{176}Lu/^{175}Lu = 0.02656$ (Blichert-Toft et al., 1997) was used for interference corrections of $^{176}Lu$ on $^{176}Hf$ assuming their fractionation are identical. Interference of $^{176}Yb$ on $^{176}Hf$ was corrected using mass bias obtained on-line and assuming $^{176}Yb/^{173}Yb = 0.79639$ (Fisher et al., 2014). Zircon 91500 was served as the external standard. Zircon GJ-1 and TEM were analyzed as unknown together with measuring samples to monitor

external uncertainties of LA-MC-ICPMS Hf measurements calibrated against 91500 standards.

### 3.3. Major and trace elements

After petrographic examination, the least-altered samples were selected for geochemical and Sr–Nd isotope analyses. Major element oxides were analyzed using a RANalytical Axios-advance (Axios PW4400) X-ray fluorescence spectrometer at the State Key Laboratory of Ore Deposit Geochemistry, Institute of Geochemistry, Chinese Academy of Sciences (IGCAS) on fused glass beads. The fused glass beads were used and the analytical precision, as determined on the Chinese National standard GSR-1 and GSR-3, and analytical uncertainties are between 1% and 5%. Loss on ignition (LOI) was obtained using 1 g of powder heated at 1100 °C for 1 h.

Trace elements were analyzed using a Perkin-Elmer Sciex ELAN 6000 inductively coupled plasma mass spectrometer (ICP-MS) at

IGCAS. Analytical procedures are similar to those described by Qi et al. (2000). About 50 mg of each powdered sample was dissolved in a high-pressure Teflon bomb for 48 h at ca. 190 °C using a HF + HNO₃ mixture. An internal standard solution containing the single element Rh was used to monitor signal drift during counting. The international standard, GBPG-1 was used for analytical quality control, and analytical precision was better than 5% for all elements.

### 3.4. Whole-rock Sr–Nd isotopic compositions

Sr–Nd isotopic ratios were measured on a subset of whole-rock samples using a Finnigan MAT-261 thermal ionization mass spectrometer (TIMS) at Tianjin Institute of Geology and Mineral Resources, China Geological Survey, following procedures similar to those of Jahn et al. (1996). The powders were treated with 0.3 N HCl for 1 h at about 100 °C and dried after rinsing with purified water. The sample were weight and spiked with mixed isotope tracers, dissolved in Teflon capsules with Hf + HNO₃ mixture at 120 °C for 7 days. Procedural blanks were <60 pg for Sm and Nd and <600 pg for Rb and Sr. Mass fractionation corrections for Sr and Nd isotopic rations were based on $^{86}Sr/^{88}Sr = 0.1194$ and $^{146}Nd/^{144}Nd = 0.7129$, respectively.

## 4. Results

### 4.1. SIMS zircon U–Pb dating

Zircons from samples SKS-31 and SKS-36 have similar morphology and internal structures under CL. Most grains are euhedral, transparent, and colorless. They are 150–300 μm in length with aspect ratios between 2:1 and 4:1. Euhedral concentric zoning is common in most crystals under CL. They locally contain inherited cores and mineral inclusions (Fig. 4a).

Twenty-four analytical spots were conducted on 23 zircon grains from sample SKS-31 (Table 1). They have a relatively constant U (243–761 ppm) and Th (93–476 ppm) with Th/U of 0.30–1.17. Their common Pb ($f_{206}$) is lower than 0.3%. Most analyses yielded a concordant age of 158.3 ± 1.2 Ma (2σ, MSWD of concordance = 0.004), which is identical to the weighted mean $^{206}Pb/^{238}U$ age of 158.2 ± 1.6 Ma (n = 23, MSWD = 0.77). One core analysis (SKS-31@18) yielded an older $^{206}Pb/^{238}U$ age of 744.8 ± 10.6 Ma (1σ) (Fig. 4b).

### 4.2. Major and trace elements geochemical characteristics

Rocks from Shuikoushan intrusion have a wide range of SiO₂ (58.4–65.2 wt.%), FeO(Total) (3.65–6.68 wt.%), and MgO (2.31–3.19 wt.%). They have a relatively high Al₂O₃ (15.0–17.2%), Sr (>400 ppm, two samples exceptions), and Ba (579–805 ppm) concentrations. They also display high total alkalis contents (K₂O + Na₂O = 5.60–7.55%) with K₂O/Na₂O ratios of 1.07–1.87, and low Rr/Sr (0.21–1.25) ratios (Table 2). Therefore, rocks from the Shuikoushan intrusion are plotted predominantly in the granodiorite field (Fig. 5a) and fall in the domains of high-K calc-alkaline series and shoshonitic series (Fig. 6h). Their A/CNK values range from 0.97 to 1.23 with an average value of 1.04, and thus plot predominantly in the prealuminous field (Fig. 5b). Furthermore, their Al₂O₃, FeO(Total), MgO, CaO, TiO₂, and P₂O₅ concentrations are negatively correlated with SiO₂. However, they have constant Na₂O, K₂O and MnO contents (Fig. 6).

The Shuikoushan granitoids have moderate rare earth element (REE) contents (∑REE = 154–222 ppm) (Table 2). Their chondrite-normalized REE patterns show steep LREE ([La/Sm]ₙ = 3.47–5.19) and relatively flat HREE patterns ([Gd/Yb]ₙ = 1.47–3.33) with weak
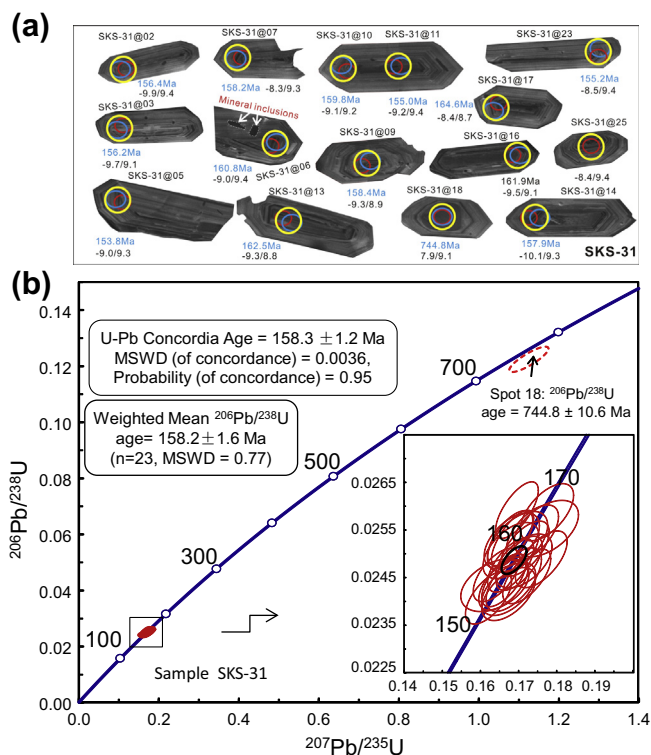


**Fig. 4.** CL images of representative zircons analyzed for *in situ* U–Pb, Hf, and O isotopes (a) and U–Pb Concordia diagram for zircon from the Shuikoushan granodiorites (b). Notes: Blue and red ellipses indicate the SIMS analyzing spots for U–Pb and O isotopes, respectively. Yellow large circles denote the LA-MC-ICPMS analyzing spots for Hf isotopes. White dashes denote the mineral inclusions in zircons. Numbers near the analyzing spots are the U–Pb ages and $\varepsilon_{Hf}(t)/\delta^{18}O$ values. (For interpretation of the references to color in this figure legend, the reader is referred to the web version of this article.)

negative Eu anomalies (Eu/Eu* = 0.73–0.95) (Fig. 7a). In the primitive mantle-normalized trace element diagram, all samples exhibit strong negative Nb–Ta–Ti, Ba, and Sr anomalies and positive Rb, Th, U, La (LREE), K, and Pb anomalies (Fig. 8a).

Compared with the other granitoids in this region, such as the Baoshan granitoids and Tongshanling granitoids (Wang et al., 2003a), the Shuikoushan granitoids have a relatively low SiO₂ concentration, but high MgO, FeO(Total), Al₂O₃, TiO₂, P₂O₅ (Fig. 6), compatible element (Ni, Co and Sc), and LREE contents. Rocks from Shuikoushan intrusion are also significantly different from neighboring contemporaneity peraluminous S-type granitoids (e.g., Xihuashan and Yaogangxian) (Figs. 6, 8b and 9b). These geochemical characteristics indicate that the Shuikoushan granitoid intrusion had a unique forming mechanism.

### 4.3. Sr–Nd isotopic composition

Rocks from the Shuikoushan intrusion have restricted present-day $^{87}Sr/^{86}Sr$ (0.711820–0.711864) and $^{143}Nd/^{144}Nd$ (0.512120–0.512131) ratios. Their age-corrected initial $^{87}Sr/^{86}Sr$ ($I_{Sr}$) ratios range from 0.7101 to 0.7102 (Table 3); and $\varepsilon_{Nd}(t)$ values range from −5.92 to −6.13. Their two-stage Nd model ages ($T_{2DM}$) are mostly between 1.43 and 1.44 Ga (Table 3). These Sr–Nd isotopic values are the same as those previous reported ($\varepsilon_{Nd}$(158.3 Ma) = −5.81 to −6.08) (Wang et al., 2003a). Compared with the Tongshanling and Baoshan granitoids, Shuikoushan granitoids show homogeneous Sr–Nd isotopic compositions (Fig. 9a).

**Table 1**
SIMS zircon U–Pb isotopic data for the Shuikoushan granodiorites (sample SKS-31).

| Sample/spot # | U (ppm) | Th (ppm) | Th/U ratio | $f_{206}$ (%) | $^{207}Pb/^{235}U$ | ±1σ (%) | $^{206}Pb/^{238}U$ | ±1σ (%) | $^{207}Pb/^{206}Pb$ | ±1σ (%) | $t_{207/206}$ (Ma) | ±1σ (Ma) | $t_{207/235}$ (Ma) | ±1σ (Ma) | $t_{206/238}$ (Ma) | ±1σ (Ma) |
|---|---|---|---|---|---|---|---|---|---|---|---|---|---|---|---|---|
| SKS-31@01 | 298 | 170 | 0.742 | 0.33 | 0.16789 | 2.88 | 0.0251 | 1.56 | 0.04859 | 2.42 | 159.7 | 2.5 | 157.6 | 4.2 | 159.6 | 2.5 |
| SKS-31@02 | 447 | 267 | 0.776 | 0.22 | 0.16421 | 2.44 | 0.0246 | 1.50 | 0.04851 | 1.93 | 156.5 | 2.3 | 154.4 | 3.5 | 156.4 | 2.3 |
| SKS-31@03 | 464 | 215 | 0.312 | 0.00 | 0.17205 | 2.40 | 0.0245 | 1.54 | 0.05089 | 1.84 | 155.8 | 2.4 | 161.2 | 3.6 | 156.2 | 2.4 |
| SKS-31@04 | 393 | 194 | 0.400 | 0.31 | 0.16870 | 2.81 | 0.0245 | 1.79 | 0.05003 | 2.17 | 155.6 | 2.8 | 158.3 | 4.1 | 155.8 | 2.8 |
| SKS-31@05 | 388 | 234 | 0.453 | 0.00 | 0.16729 | 2.77 | 0.0241 | 1.53 | 0.05025 | 2.31 | 153.6 | 2.3 | 157.1 | 4.0 | 153.8 | 2.3 |
| SKS-31@06 | 413 | 207 | 0.591 | 0.00 | 0.16972 | 3.04 | 0.0253 | 1.65 | 0.04874 | 2.55 | 160.9 | 2.6 | 159.2 | 4.5 | 160.8 | 2.6 |
| SKS-31@07 | 761 | 456 | 0.487 | 0.04 | 0.17128 | 2.86 | 0.0248 | 1.51 | 0.05001 | 2.42 | 158.0 | 2.4 | 160.5 | 4.3 | 158.2 | 2.4 |
| SKS-31@08 | 547 | 300 | 0.523 | 0.11 | 0.16610 | 2.29 | 0.0244 | 1.50 | 0.04929 | 1.73 | 155.6 | 2.3 | 156.0 | 3.3 | 155.7 | 2.3 |
| SKS-31@09 | 462 | 209 | 0.297 | 0.04 | 0.17584 | 2.56 | 0.0249 | 1.60 | 0.05126 | 2.00 | 158.0 | 2.5 | 164.5 | 3.9 | 158.4 | 2.5 |
| SKS-31@10 | 523 | 225 | 0.396 | 0.00 | 0.17148 | 2.47 | 0.0251 | 1.52 | 0.04954 | 1.95 | 159.8 | 2.4 | 160.7 | 3.7 | 159.8 | 2.4 |
| SKS-31@11 | 426 | 167 | 0.428 | 0.35 | 0.16376 | 3.58 | 0.0243 | 1.50 | 0.04880 | 3.25 | 155.1 | 2.3 | 154.0 | 5.1 | 155.0 | 2.3 |
| SKS-31@12 | 424 | 287 | 0.748 | 0.07 | 0.16208 | 2.44 | 0.0241 | 1.51 | 0.04883 | 1.92 | 153.4 | 2.3 | 152.5 | 3.5 | 153.4 | 2.3 |
| SKS-31@13 | 243 | 93 | 0.315 | 0.00 | 0.17721 | 3.11 | 0.0255 | 1.52 | 0.05035 | 2.72 | 162.3 | 2.5 | 165.7 | 4.8 | 162.5 | 2.4 |
| SKS-31@14 | 482 | 175 | 0.295 | 0.00 | 0.17005 | 2.34 | 0.0248 | 1.52 | 0.04974 | 1.78 | 157.8 | 2.4 | 159.5 | 3.5 | 157.9 | 2.4 |
| SKS-31@15 | 564 | 239 | 0.667 | 0.09 | 0.16772 | 2.33 | 0.0253 | 1.51 | 0.04803 | 1.78 | 161.5 | 2.4 | 157.4 | 3.4 | 161.2 | 2.4 |
| SKS-31@16 | 477 | 210 | 0.444 | 0.15 | 0.17350 | 2.61 | 0.0254 | 1.54 | 0.04948 | 2.11 | 161.9 | 2.5 | 162.4 | 3.9 | 161.9 | 2.5 |
| SKS-31@17 | 528 | 282 | 0.491 | 0.00 | 0.17731 | 2.61 | 0.0259 | 1.55 | 0.04971 | 2.10 | 164.6 | 2.5 | 165.7 | 4.0 | 164.6 | 2.5 |
| SKS-31@18 | 391 | 255 | 0.553 | 0.10 | 1.12558 | 1.77 | 0.1225 | 1.50 | 0.06665 | 0.94 | 742.4 | 10.8 | 765.6 | 9.6 | 744.8 | 10.6 |
| SKS-31@19 | 445 | 163 | 0.306 | 0.07 | 0.16727 | 2.81 | 0.0243 | 1.53 | 0.05002 | 2.36 | 154.3 | 2.3 | 157.0 | 4.1 | 154.5 | 2.3 |
| SKS-31@20 | 679 | 476 | 1.034 | 0.04 | 0.16835 | 2.17 | 0.0253 | 1.56 | 0.04824 | 1.50 | 161.4 | 2.5 | 158.0 | 3.2 | 161.1 | 2.5 |
| SKS-31@21 | 690 | 344 | 1.172 | 0.00 | 0.16952 | 2.18 | 0.0259 | 1.52 | 0.04744 | 1.56 | 165.3 | 2.5 | 159.0 | 3.2 | 164.9 | 2.5 |
| SKS-31@22 | 487 | 206 | 0.413 | 0.00 | 0.16788 | 2.35 | 0.0248 | 1.50 | 0.04918 | 1.81 | 157.7 | 2.4 | 157.6 | 3.4 | 157.7 | 2.3 |
| SKS-31@23 | 443 | 282 | 0.586 | 0.07 | 0.16596 | 2.56 | 0.0244 | 1.51 | 0.04940 | 2.07 | 155.1 | 2.5 | 155.9 | 3.7 | 155.2 | 2.3 |
| SKS-31@24 | 402 | 250 | 0.957 | 0.08 | 0.16809 | 2.85 | 0.0253 | 1.54 | 0.04825 | 2.40 | 161.1 | 2.5 | 157.8 | 4.2 | 160.9 | 2.4 |

Note: $f_{206}$ is the percentage of common $^{206}Pb$ in total $^{206}Pb$.

### 4.4. Zircon Hf–O isotope

*In situ* Hf and O isotopic analyses were conducted on zircon grains from samples SKS-31 and SKS-36 (Table 4). Zircons from sample SKS-31 have fairly homogenous Hf and O isotopic compositions. Their present $^{176}Hf/^{177}Hf$ ranges from 0.282391 to 0.282449, corresponding to $\varepsilon_{Hf}(t)$ from −10.2 to −8.1. They have high zircon $\delta^{18}O$ (8.7–9.4‰) and middle Paleoproterozoic Hf two-stage model ages ($T_{2DM}$ = 1.7–1.9 Ga). The measured Hf and O isotopes form a normal Gaussian distribution and yield low average $\varepsilon_{Hf}(t)$ values of −9.1 ± 0.2 (2σ) (Fig. 10a) and a high average of $\delta^{18}O$ values 9.2‰ ± 0.1‰ (2σ) (Fig. 10b). Similarly, zircons from sample SKS-36 also show relatively homogenous Hf and O isotopic compositions. Their $^{176}Hf/^{177}Hf$ varies from 0.282376 to 0.282470, corresponding to $\varepsilon_{Hf}(t)$ = −10.6 to −7.4 and $T_{2DM}$ = 1.7–1.9 Ga. The normal distribution existed with an average of $\varepsilon_{Hf}(t)$ value of −8.7 ± 0.3 (2σ) (Fig. 10c). They also have a high and constant $\delta^{18}O$ value (8.4‰ and 9.7‰) with an average of $\delta^{18}O$ = 9.1‰ ± 0.2‰ (2σ) (Fig. 10d).

## 5. Discussions

This study, together with previous data (Ma et al., 2006; Wang et al., 2002, 2003a; Zuo, 2014), shows that rocks from Shuikoushan granitoid intrusion have the following characteristic features of elements and isotope geochemistry: (1) fractionated REE patterns with low HREE contents, negative high-field-strength elements (HFSE) anomalies (Nb, Ta, and Ti), and positive anomalies in Pb and K (Figs. 7 and 9); (2) a late Jurassic age of 158 Ma for magmatic activity, Neoproterozoic age for the inherited zircon cores (745 Ma) (Fig. 4b), and middle Paleoproterozoic Hf two-stage model ages (1.7–1.9 Ga); (3) moderately high initial $^{87}Sr/^{86}Sr$ ratios of 0.7101–0.7102 and negative $\varepsilon_{Nd}(t)$ values of −5.92 to −6.13; and (4) relatively homogeneous high zircon $\delta^{18}O$ ratios of 8.4‰ to 9.7‰ and negative $\varepsilon_{Hf}(t)$ values of −10.6 to −8.1. These new findings were used to examine the interrelated magmatic and tectonic processes that have resulted in these distinguishing characteristics of Shuikoushan granitoids as compared with other granitoids in the adjacent region.

### 5.1. Genetic type: I-type or S-type?

Based on chemical and mineralogical criteria, granitoid rocks are classified as I-, S-, A-, and M types (Chappell and White, 1974; White and Chappell, 1983; Whalen, 1985; Whalen et al., 1987). The Shuikoushan granitoids show high initial $^{87}Sr/^{86}Sr$ ratios (0.7101–0.7102) and negative $\varepsilon_{Nd}(t)$ values (−5.92 to −6.13). They also have negative zircon $\varepsilon_{Hf}(t)$ (−10.6 to −8.1) and high $\delta^{18}O$ (8.4–9.7‰) values that are substantially different from rocks from mantle sources. Therefore, they are not M-type granitoids that are generally derived from mantle source or formed by the partial melting of juvenile crust (Whalen, 1985).

A-type granitoid typically contains high-temperature anhydrous minerals, such as pyroxene, fayalite, and interstitial (late-crystallizing) biotite and amphibole (King et al., 1997). Feldspar from A-type granitoid is mainly alkali feldspar, commonly albite–orthoclase solid solutions or intergrowths (Collins et al., 1982). Additionally, micrographic intergrowth of quartz and alkali feldspar is very common (Collins et al., 1982; Whalen et al., 1987). A-type granitoids are characterized by the enrichment of the HFSE and REE concentrations with Zr higher than 250 ppm and Zr + Nb + Ce + Y higher than 350 ppm (Collins et al., 1982; Whalen et al., 1987). Rocks from the Shuikoushan intrusion were previously considered as A-type granitoids (Jin and Luo, 2012). However, the Shuikoushan granitoids contain biotite and hornblende which are not interstitial minerals (Fig. 3). In addition, they do not have pyroxene or fayalite. Typical mineral assemblage of A-type granitoid has not been identified in Shuikoushan granitoids (Fig. 3). They also have relatively low Zr, Nb, Ce, and Y contents (Fig. 11). The mineral assemblage and chemical composition indicate that rocks from the Shuikoushan intrusion are not A-type granitoids.

S-type granitoids generally contain Al-rich minerals, such as cordierite or muscovite, whereas I-type granitoids always contain hornblende, especially at the more mafic end of the compositional

**Table 2**
Major (wt.%) and trace element (ppm) data for the Shuikoushan granodiorites.

| Sample | SKS-6 | SKS-15 | SKS-16 | SKS-29 | SKS-30 | SKS-31 | SKS-32 | SKS-33 | SKS-35 | SKS-36 | SKS-37 | SKS-50 | SKS-123 | SKS-124 | SKS-125 |
|---|---|---|---|---|---|---|---|---|---|---|---|---|---|---|---|
| *Major element (wt.%)* | | | | | | | | | | | | | | | |
| $SiO_2$ | 62.3 | 62.4 | 65.2 | 62.1 | 63.7 | 64.4 | 62.8 | 62.0 | 62.0 | 62.3 | 62.1 | 62.2 | 59.6 | 60.6 | 58.4 |
| $Al_2O_3$ | 15.8 | 16.0 | 15.0 | 15.7 | 15.4 | 16.0 | 15.4 | 16.1 | 15.8 | 15.7 | 15.5 | 15.8 | 16.2 | 17.0 | 17.2 |
| $Fe_2O_3^T$ | 6.21 | 5.09 | 4.06 | 6.27 | 5.04 | 6.12 | 5.80 | 6.51 | 5.28 | 6.04 | 5.66 | 6.08 | 7.42 | 6.72 | 7.26 |
| MgO | 2.59 | 2.76 | 2.09 | 2.58 | 3.19 | 2.67 | 2.51 | 2.38 | 2.29 | 2.90 | 2.38 | 2.46 | 2.53 | 2.44 | 2.32 |
| CaO | 3.65 | 1.50 | 2.04 | 3.65 | 2.87 | 3.43 | 4.10 | 3.30 | 4.18 | 3.43 | 4.64 | 3.46 | 5.01 | 3.90 | 2.94 |
| $Na_2O$ | 2.91 | 3.58 | 2.66 | 3.06 | 2.65 | 3.18 | 2.50 | 3.05 | 3.32 | 3.42 | 3.26 | 3.43 | 3.30 | 2.29 | 2.12 |
| $K_2O$ | 4.00 | 3.97 | 4.85 | 4.02 | 4.00 | 3.98 | 3.10 | 3.88 | 3.55 | 3.77 | 3.62 | 4.07 | 2.78 | 4.29 | 5.17 |
| MnO | 0.09 | 0.08 | 0.06 | 0.09 | 0.06 | 0.10 | 0.11 | 0.12 | 0.07 | 0.07 | 0.09 | 0.08 | 0.11 | 0.08 | 0.07 |
| $TiO_2$ | 0.70 | 0.68 | 0.57 | 0.70 | 0.70 | 0.74 | 0.71 | 0.76 | 0.70 | 0.70 | 0.71 | 0.69 | 0.78 | 0.86 | 0.89 |
| $P_2O_5$ | 0.42 | 0.28 | 0.27 | 0.41 | 0.34 | 0.36 | 0.35 | 0.37 | 0.34 | 0.34 | 0.34 | 0.34 | 0.41 | 0.44 | 0.52 |
| L.O.I. | 2.93 | 2.83 | 4.71 | 2.05 | 3.91 | 2.27 | 4.24 | 3.06 | 3.63 | 2.78 | 3.17 | 2.82 | 2.90 | 2.41 | 3.11 |
| Total | 101.5 | 99.1 | 101.5 | 100.6 | 101.3 | 101.3 | 101.5 | 101.5 | 101.1 | 101.4 | 101.5 | 101.5 | 101.0 | 101.0 | 100.0 |
| $K_2O/Na_2O$ | 1.37 | 1.11 | 1.82 | 1.31 | 1.51 | 1.25 | 1.24 | 1.27 | 1.07 | 1.10 | 1.11 | 1.19 | 0.84 | 1.87 | 2.44 |
| A/CNK | 1.00 | 1.23 | 1.13 | 0.98 | 1.10 | 1.01 | 1.03 | 1.06 | 0.93 | 0.98 | 0.98 | 0.97 | 0.98 | 1.09 | 1.19 |
| $K_2O + Na_2O$ | 6.91 | 7.55 | 7.51 | 7.07 | 6.65 | 7.16 | 5.60 | 6.93 | 6.87 | 7.18 | 6.88 | 7.51 | 6.08 | 6.58 | 7.29 |
| $Mg^\#$ | 0.32 | 0.38 | 0.36 | 0.31 | 0.41 | 0.33 | 0.32 | 0.29 | 0.33 | 0.35 | 0.32 | 0.31 | 0.27 | 0.29 | 0.26 |
| *Trace element (ppm)* | | | | | | | | | | | | | | | |
| Sc | 16.6 | 13.1 | 15.2 | 15.6 | 15.5 | 17.4 | 14.4 | 15.5 | 15.2 | 16.3 | 16.8 | 16.7 | 18.0 | 17.8 | 20.3 |
| V | 135 | 108 | 118 | 129 | 123 | 142 | 115 | 134 | 130 | 131 | 135 | 135 | 138 | 152 | 180 |
| Cr | 43.0 | 32.6 | 57.1 | 35.0 | 32.9 | 40.3 | 30.2 | 35.6 | 36.4 | 35.7 | 37.4 | 36.1 | 30.8 | 29.6 | 42.0 |
| Co | 180 | 109 | 165 | 145 | 168 | 133 | 134 | 143 | 178 | 139 | 145 | 142 | 101 | 99.5 | 60.0 |
| Ni | 14.7 | 12.5 | 21.0 | 11.9 | 9.6 | 12.0 | 11.1 | 11.8 | 12.4 | 12.5 | 11.2 | 10.7 | 10.6 | 10.7 | 12.4 |
| Cu | 25.5 | 201.8 | 123.8 | 31.4 | 81.9 | 32.6 | 471 | 12.1 | 17.4 | 10.8 | 27.9 | 13.2 | 45.0 | 38.9 | 75.6 |
| Zn | 90.8 | 71.7 | 81.5 | 97.2 | 102.5 | 101.7 | 64.8 | 63.6 | 103.8 | 62.6 | 89.8 | 83.2 | 90.0 | 71.1 | 72.3 |
| Ga | 19.2 | 18.4 | 19.8 | 18.2 | 19.0 | 19.6 | 18.3 | 19.5 | 18.7 | 19.0 | 18.4 | 19.7 | 18.5 | 19.5 | 17.5 |
| Ge | 1.57 | 1.54 | 1.35 | 1.58 | 1.46 | 1.52 | 1.39 | 1.38 | 1.32 | 1.47 | 1.38 | 1.59 | 1.62 | 1.61 | 1.31 |
| As | 12.36 | 11.99 | 12.26 | 12.01 | 12.33 | 12.37 | 12.65 | 12.27 | 12.35 | 12.74 | 12.89 | 12.73 | 1.75 | 1.87 | 2.14 |
| Rb | 132 | 168 | 144 | 107 | 147 | 135 | 224 | 116 | 112 | 114 | 112 | 133 | 99 | 157 | 165 |
| Sr | 491 | 356 | 309 | 494 | 442 | 510 | 180 | 426 | 446 | 441 | 465 | 491 | 478 | 450 | 198 |
| Y | 24.6 | 24.0 | 21.2 | 23.9 | 23.0 | 24.8 | 24.4 | 21.4 | 21.4 | 22.9 | 23.9 | 24.7 | 26.3 | 25.1 | 24.0 |
| Zr | 132 | 139 | 152 | 136 | 133 | 124 | 156 | 130 | 151 | 129 | 127 | 141 | 129 | 125 | 117 |
| Nb | 14.6 | 15.6 | 16.9 | 14.6 | 14.2 | 14.5 | 15.1 | 15.1 | 14.5 | 14.6 | 14.7 | 14.8 | 14.1 | 15.7 | 14.0 |
| Mo | 1.63 | 2.03 | 69.43 | 2.48 | 1.35 | 1.45 | 1.02 | 3.12 | 2.86 | 3.32 | 1.46 | 1.23 | 0.91 | 1.00 | 0.72 |
| Cs | 5.16 | 5.72 | 6.14 | 4.01 | 5.65 | 5.89 | 12.14 | 3.57 | 4.29 | 3.62 | 4.32 | 5.70 | 6.27 | 19.30 | 14.20 |
| Ba | 729 | 710 | 777 | 645 | 660 | 729 | 664 | 579 | 619 | 591 | 630 | 681 | 607 | 758 | 805 |
| Hf | 3.69 | 4.00 | 4.01 | 3.76 | 3.49 | 3.37 | 4.11 | 3.69 | 4.12 | 3.82 | 3.71 | 3.95 | 3.59 | 3.65 | 3.23 |
| Ta | 0.92 | 1.08 | 1.05 | 0.96 | 0.90 | 0.82 | 0.87 | 0.95 | 0.91 | 0.98 | 0.96 | 0.96 | 1.60 | 2.14 | 1.50 |
| Pb | 39.9 | 16.4 | 8.7 | 27.3 | 67.8 | 27.6 | 9.6 | 29.6 | 20.9 | 35.3 | 21.9 | 23.2 | 16.9 | 22.5 | 12.8 |
| Th | 13.3 | 17.6 | 13.1 | 12.7 | 12.4 | 10.4 | 12.3 | 13.5 | 12.5 | 14.1 | 13.2 | 13.8 | 12.6 | 12.6 | 9.56 |
| U | 2.97 | 4.04 | 3.29 | 3.27 | 3.05 | 2.45 | 2.71 | 3.16 | 2.96 | 3.32 | 2.84 | 3.19 | 2.40 | 4.00 | 2.95 |
| La | 43.0 | 44.3 | 40.2 | 36.6 | 37.2 | 36.6 | 38.8 | 35.2 | 38.3 | 39.2 | 37.4 | 43.0 | 45.5 | 46.3 | 47.5 |
| Ce | 79.1 | 78.9 | 72.1 | 68.5 | 68.7 | 69.3 | 71.6 | 62.5 | 70.9 | 72.2 | 70.1 | 81.7 | 88.7 | 93.4 | 92.5 |
| Pr | 9.30 | 8.92 | 8.14 | 8.09 | 8.15 | 8.49 | 8.54 | 7.58 | 8.35 | 8.62 | 8.44 | 9.50 | 10.7 | 11.0 | 10.8 |
| Nd | 34.0 | 31.7 | 29.6 | 30.0 | 29.8 | 32.5 | 31.6 | 28.1 | 30.5 | 31.9 | 30.6 | 34.6 | 40.9 | 40.4 | 43.2 |
| Sm | 6.38 | 5.94 | 5.56 | 5.74 | 5.83 | 6.44 | 6.16 | 5.49 | 5.63 | 6.13 | 5.99 | 6.49 | 7.96 | 7.05 | 7.87 |
| Eu | 1.66 | 1.58 | 1.41 | 1.51 | 1.53 | 1.62 | 1.36 | 1.43 | 1.46 | 1.48 | 1.49 | 1.63 | 2.25 | 1.82 | 1.72 |
| Gd | 4.82 | 4.54 | 4.09 | 4.29 | 4.41 | 4.69 | 4.50 | 4.00 | 4.05 | 4.21 | 4.23 | 4.70 | 6.60 | 5.81 | 6.69 |
| Tb | 0.87 | 0.81 | 0.74 | 0.79 | 0.80 | 0.85 | 0.86 | 0.73 | 0.76 | 0.83 | 0.84 | 0.90 | 1.06 | 0.88 | 0.94 |
| Dy | 4.39 | 4.08 | 3.75 | 4.06 | 4.01 | 4.27 | 4.42 | 3.72 | 3.73 | 4.17 | 4.45 | 4.45 | 5.23 | 4.62 | 4.71 |
| Ho | 0.94 | 0.92 | 0.81 | 0.87 | 0.84 | 0.92 | 0.95 | 0.80 | 0.82 | 0.92 | 0.94 | 0.96 | 1.05 | 0.94 | 0.90 |
| Er | 2.50 | 2.43 | 2.16 | 2.33 | 2.27 | 2.45 | 2.57 | 2.09 | 2.15 | 2.43 | 2.49 | 2.51 | 2.89 | 2.85 | 2.44 |
| Tm | 0.35 | 0.35 | 0.31 | 0.34 | 0.31 | 0.34 | 0.35 | 0.29 | 0.30 | 0.35 | 0.36 | 0.35 | 0.43 | 0.41 | 0.35 |
| Yb | 2.30 | 2.34 | 2.11 | 2.24 | 2.02 | 2.19 | 2.26 | 1.92 | 1.97 | 2.28 | 2.39 | 2.38 | 2.65 | 2.66 | 2.09 |
| Lu | 0.34 | 0.34 | 0.31 | 0.34 | 0.30 | 0.33 | 0.33 | 0.28 | 0.29 | 0.33 | 0.36 | 0.35 | 0.39 | 0.40 | 0.29 |
| $\sum$REE | 190 | 187 | 171 | 166 | 166 | 171 | 174 | 154 | 169 | 175 | 170 | 194 | 216 | 219 | 222 |
| $[La/Sm]_N$ | 4.35 | 4.82 | 4.67 | 4.11 | 4.11 | 3.66 | 4.06 | 4.13 | 4.39 | 4.13 | 4.03 | 4.27 | 3.69 | 4.24 | 3.90 |
| $[Gd/Yb]_N$ | 1.73 | 1.60 | 1.60 | 1.58 | 1.81 | 1.78 | 1.65 | 1.73 | 1.70 | 1.52 | 1.47 | 1.63 | 2.06 | 1.81 | 2.65 |
| $[La/Yb]_N$ | 13.4 | 13.6 | 13.7 | 11.7 | 13.2 | 12.0 | 12.3 | 13.2 | 13.9 | 12.3 | 11.2 | 13.0 | 12.3 | 12.5 | 16.3 |
| $Eu/Eu^*$ | 0.92 | 0.93 | 0.90 | 0.93 | 0.92 | 0.90 | 0.79 | 0.93 | 0.94 | 0.89 | 0.91 | 0.90 | 0.95 | 0.87 | 0.73 |
| Rb/Sr | 0.27 | 0.47 | 0.47 | 0.22 | 0.33 | 0.26 | 1.25 | 0.27 | 0.25 | 0.26 | 0.24 | 0.27 | 0.21 | 0.35 | 0.83 |

Note: $Mg^\# = Mg/(Mg + Fe^{2+})$, $FeO^T = 0.8998 \times Fe_2O_3^T$. Total iron as $Fe_2O_3^T$. A/CNK = molar $Al_2O_3/(CaO + Na_2O + K_2O)$.

spectrum (Chappell et al., 2012). Shuikoushan granitoids commonly contain hornblende. However, no peraluminous minerals, such as muscovite, garnet, and cordierite, have been identified in Shuikoushan granitoids (Fig. 3). There is a negative correlation between $P_2O_5$ and $SiO_2$ (Fig. 6e), which is considered as an important feature of I-type granitoids, and thus distinguishing them from S-type granitoids (Chappell and White, 1992). Some trace elements, such as Pb, also behave distinctly in the I- and S-type melts

(Fig. 6g). Their Sr–Nd isotopic compositions are similar to those of the I-type granitoids from the Lachlan Fold Belt (Fig. 9a). Therefore, it seems that the Shuikoushan granitoids are not S-type granitoids, but rather belong to the I-type. However, some samples were peraluminous and K-rich with high A/CNK (>1.0) and $K_2O/Na_2O$ (>1.0) ratios (Table 2), whereas typical I-type granitoids usually have low A/CNK and $K_2O/Na_2O$ ratios. Peraluminous I-type granitoids may result from fractional crystallization of hornblende (Cawthorn
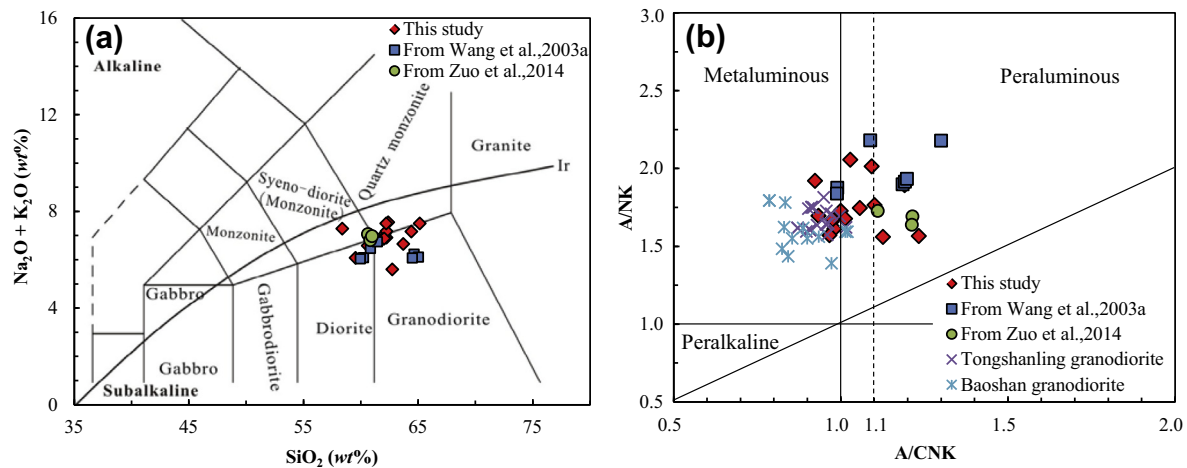
**Fig. 5.** (a) Total alkalis–SiO$_2$ diagram Middlemost (1994) for classification of rocks from the Shuikoushan granitoid intrusion. Previous reported data for the Shuikoushan granitoid intrusion are from Wang et al. (2003a) and Zuo (2014), similarly hereinafter. (b) A/NK vs. A/CNK diagram shows that the Shuikoushan granodiorites contain more Al than adjacent region other granodioritic rocks such as Tongshanling and Baoshan. Most of them display peraluminous nature. The data of Tongshanling and Baoshan granodioritic rocks are from Wang et al. (2003a), similarly hereinafter.

and Brown, 1976) or from partial melting of mafic source rocks (Chappell et al., 2012) or from crust–mantle interaction (Davis and Hawkesworth, 1993), which is discussed below.

### 5.2. Nature of the source region

Previous studies confirmed that the partial melting of supracrustal metasedimentary rocks can generate peraluminous silicic magma and form S-type granitoids (Chappell and White, 1974; Chappell et al., 2012). However, rocks from the Shuikoushan intrusion are I-type peraluminous granitoids. Their whole rock Sr–Nd and zircon Hf–O isotopic compositions are substantially different from those of granitoids derived from metasedimentary sources (Figs. 9a and 12a). Their compositions are also different from those of contemporaneous peraluminous tungsten-mineralized S-type granitoids considered to be of metasedimentary origin in the region (Figs. 6, 8b and 9b). Thus, it is impossible that the Shuikoushan peraluminous I-type granitoids were formed from the partial melting of supracrustal metasedimentary rocks. However, there are two other possibilities that may account for the origin of the Shuikoushan granitoid rocks: (1) mixing of mantle-derived mafic source and crust-derived felsic magma (Wang et al., 2001, 2003a); and (2) partial melting of mafic rocks in middle–lower crust.

Mixing between mantle and felsic magmas may result in a negative correlation of whole-rock Sr–Nd isotopes and zircon Hf–O isotopes, respectively (Li et al., 2007, 2009a). Additionally, mafic microgranular enclaves (MME) may occur in host garnitoids after mixing between mantle and felsic magmas (e.g., Barbarin, 1988). However, no mafic enclaves have been identified in the Shuikoushan granitoids. They have constant whole-rock Sr–Nd isotopes (Figs. 6j and 10a) and zircon Hf–O isotopes, respectively (Fig. 12a), indicating a relatively homogeneous source. It is unlikely that the mixing of a mafic source and felsic magmas could have yielded the Shuikoushan granitoids with homogeneous whole-rock Sr–Nd and zircon Hf–O isotopes. Moreover, the volume of mafic–ultramafic rocks in southern Hunan Province is very small, which also argues against this possibility. The Shuikoushan granitoid rocks have negative whole-rock $\varepsilon_{Nd}(t)$ (−5.92 to −6.13) and zircon $\varepsilon_{Hf}(t)$ (−10.6 to −8.1) values, which are similar to the continental lower crustal Hf and Nd isotopic compositions, respectively (Figs. 9b and 12b). Their Nd isotopic compositions are similar to those of granulite (−6.59 to −7.34) from the southern Hunan

Province and Zhejiang Province, which were considered to be representative of middle/lower crustal composition (Fig. 9a) (Kong et al., 2000; Yu et al., 2003). Thus, the middle to lower crust, as a relatively homogeneous mafic source, was strongly reworked in the late Jurassic in generating Shuikoushan peraluminous I-type granitoids.

The partial melting of mafic middle–lower crust may be proposed as a mechanism to yield the Shuikoushan granitoid intrusion. How materials can generate Shuikoushan granitoids that have high Al$_2$O$_3$ and K$_2$O contents but are of I-type rocks should be determined. It is known from experimental studies that the K content of a melt source has a significant influence on the derived melt. Meta-tholeiitic rocks have a low K$_2$O concentration that cannot yield high-K calc-alkaline melts (Roberts and Clemens, 1993). The high K$_2$O concentrations of the Shuikoushan granitoid rocks could only have been derived from a K-rich mafic source. Experiments reveal that hydrous melting of mafic rocks, such as amphibolites, can generate a peraluminous melt with high K content (Beard and Lofgren, 1991; Wolf and Wyllie, 1994; Rapp and Watson, 1995; Chappell et al., 2012). Dehydration melting of hydrous mineral-bearing mafic rocks yield water-undersaturated mildly peraluminous granodioritic melts (Beard and Lofgren, 1991; Wolf and Wyllie, 1994). Water-saturated melting of these rocks generated strong peraluminous melts enriched in Ca and depleted in Fe, Mg, and K (Beard and Lofgren, 1991). Furthermore, the Shuikoushan granitoids are characterized by high Fe, Mg, and K (Fig. 6) and low SiO$_2$ (58.4–65.2%) concentrations. Their A/CNK values range from 0.92 to 1.23 with an average value of 1.04. These characteristics are similar to those garnered by water-unsaturated dehydration melting of mafic rocks, such as amphibolites. However, residual mineral assembles after melt extraction play a crucial role in forming magmas with peculiar geochemical characteristics (Beard and Lofgren, 1991; Douce, 1999). Rocks from the Shuikoushan intrusion show fractionation of REE, flat HREE patterns, low HREE contents, and weakly negative Eu anomalies in the chondrite normalized REE patterns (Fig. 7a). Low HREE abundance and fractionated REE indicate the possible presence of garnet in the residuum after melting. However, fractionation of HREE in the Shuikoushan granitoid rocks is insignificant, as shown by their relatively flat HREE patterns (Fig. 7a). This is inconsistent with modern adakites with significant fractionation of HREE (steep HREE patterns), which are typically considered as a garnet residual in source (Martin, 1999). These plat HREE patterns suggest that
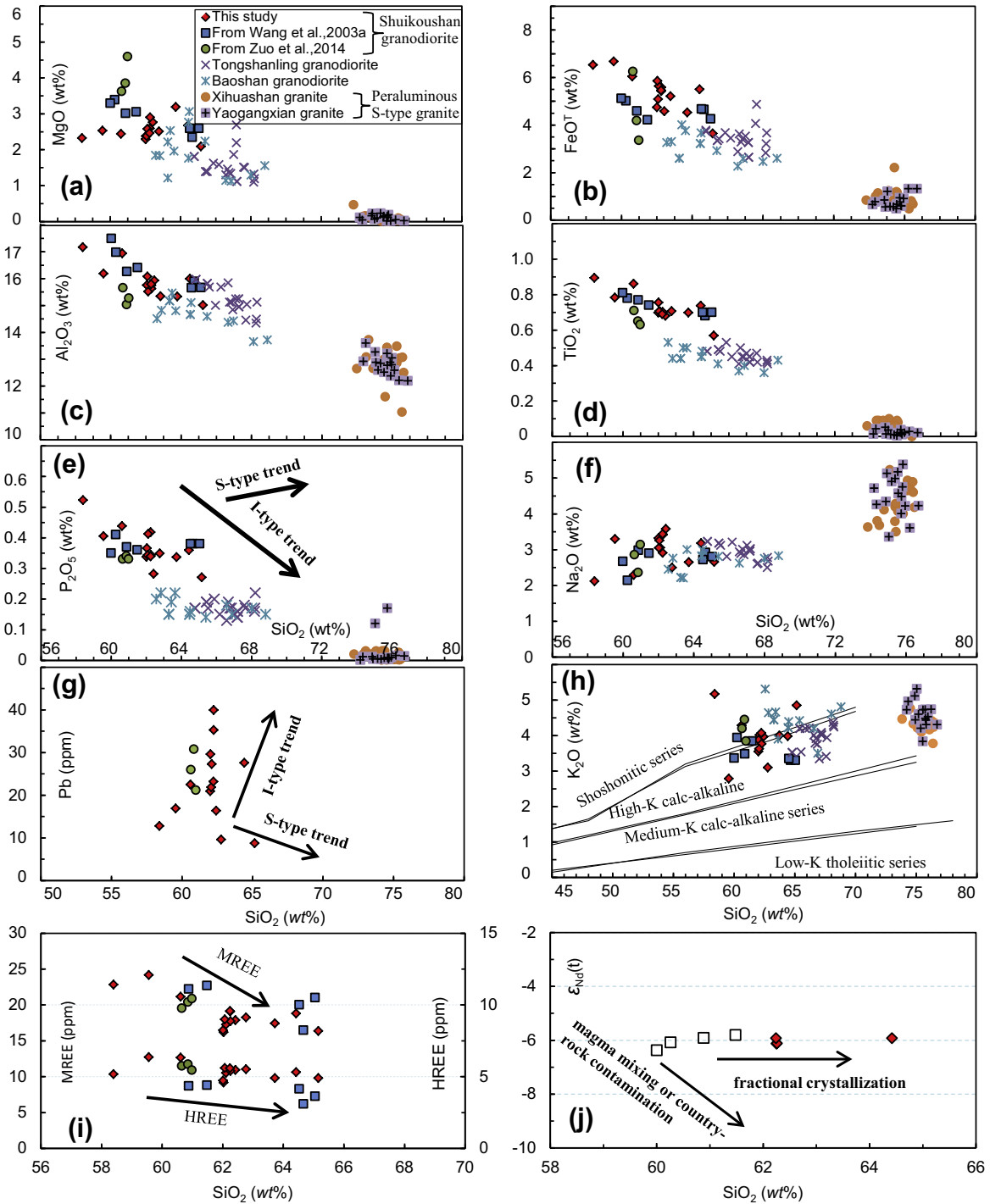
**Fig. 6.** Selected variation diagrams between major elements, trace elements, isotope and silica for the Shuikoushan granodiorites. $K_2O$ vs. $SiO_2$ classification diagram of Peccerillo and Taylor (1976) showing that these rocks extend from shoshonitic to high-K calc-alkaline in character. I-type granitoid trend is after Chappell and White (1992) and Chappell (1999). The data of Xihuashan and Yaogangxian peraluminous S-type granites are from Yang et al. (2012) and Li (2011), respectively, similarly hereinafter.

amphibole was another residual mineral during the partial melting of a mafic source. The residual amphiboles can lower the middle REE (MREE) concentrations because of its high partition coefficients ($K_D$) for these elements in intermediate to felsic melts (Arth, 1976; Bea et al., 1994). An amphibole-bearing residue for the Shuikoushan granitoids is consistent with a low $TiO_2$ concentration (Fig. 6d), low MREE contents (Fig. 7a), and low Rb/Sr ratio (Table 2). Moreover, weakly negative Eu anomalies (Fig. 7a) and insignificant Sr enrichment (Fig. 8a) relative to LREE

are observed in majority of the Shuikoushan granitoids, implying that some plagioclase may have also remained in the magma chamber (Martin, 1999). Thus, garnet, amphibole and plagioclase are major residual minerals in mafic source during dehydration melting of amphibolites.

Dehydration-melting of amphibolite has been widely experimental studied (Beard and Lofgren, 1991; Wyllie and Wolf, 1993; Wolf and Wyllie, 1994). These studies suggest that the hydrous mineral amphibole breakdown will initially supply water during
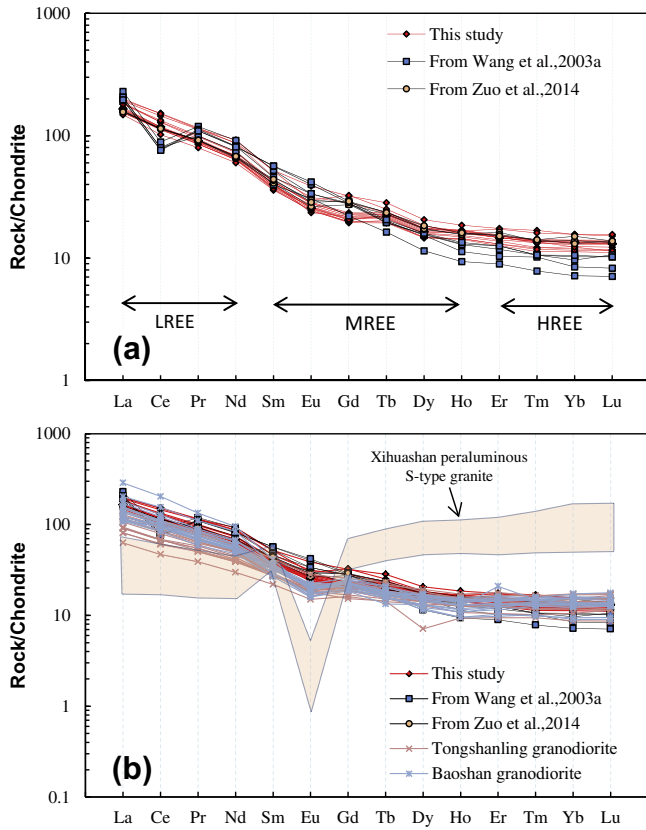
**Fig. 7.** Chondrite-normalized REE diagrams for the Shuikoushan granodiorites. The normalization values are from Sun and McDonough (1989).
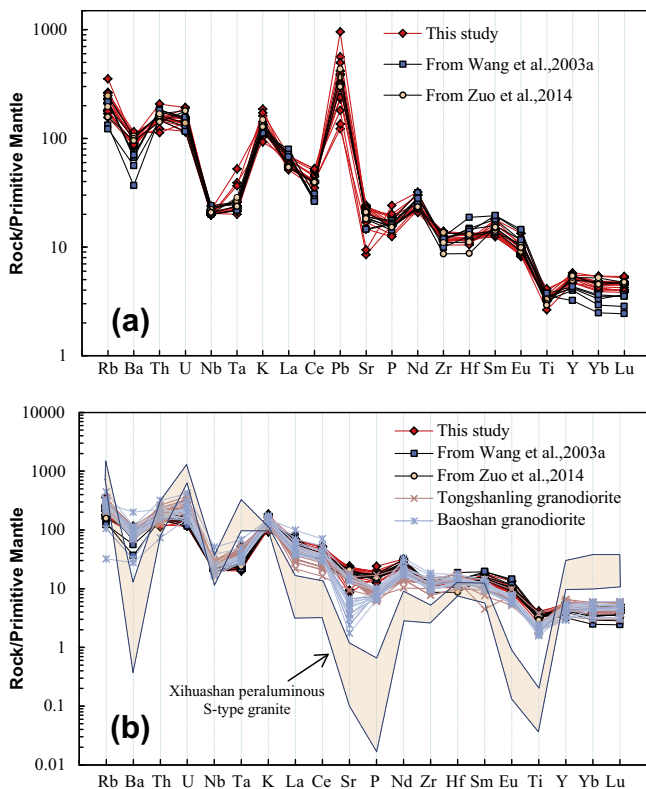


**Fig. 8.** Primitive mantle-normalized multi-element spidergrams of the Shuikoushan granodiorites. The normalization values are from Sun and McDonough (1989).
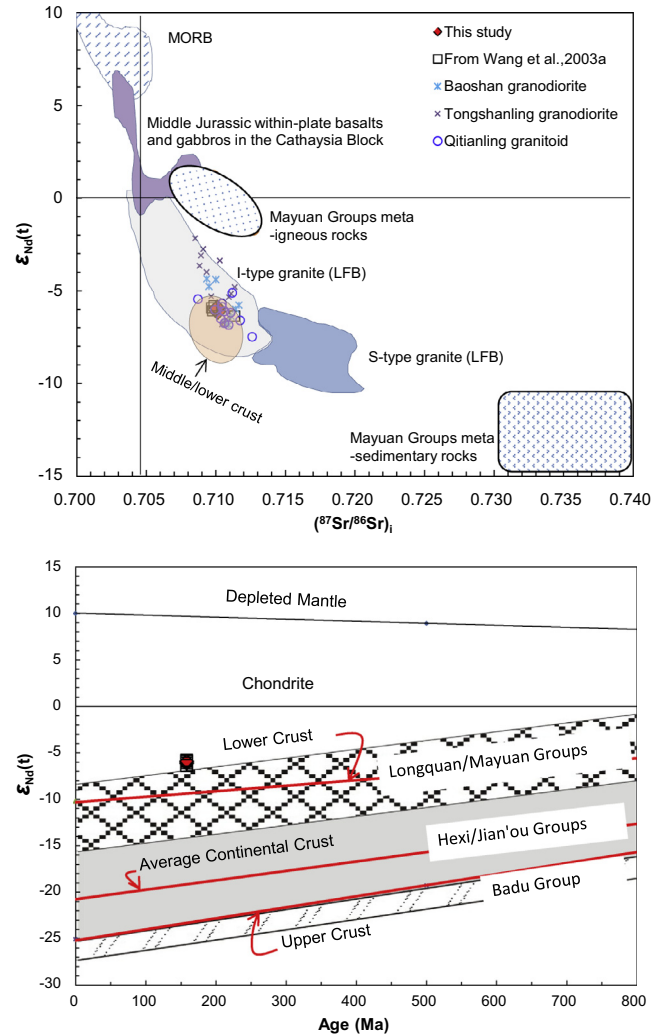


**Fig. 9.** Sr–Nd isotopic compositions of the intrusive rocks in the Shuikoushan and adjacent region. All the initial isotopic ratios were corrected to 158.3 Ma. The Sr–Nd isotopes of Shuikoushan granodiorites are similar to the Lachlan Fold Belt I-type granitoids in Australia (Healy et al., 2004) and are different from those mantle-derived Jurassic basalts and gabbros in the adjacent region (Li et al., 2003a; Wang et al., 2003b, 2006 and references therein). Compared with adjacent other granodiorites such as Tongshanling and Baoshan (Wang et al., 2003a), the Shuikoushan granodiorites have relatively homogeneous Sr–Nd isotopic compositions and are similar with Qitianling intrusion (Zhao et al., 2012). The Sr–Nd isotopic data of middle/lower crust are from Yu et al. (2003) and Kong et al. (2000). The Mayuan Groups metaigneous rocks and metasedimentary rocks are from Yuan et al. (1991). Nd isotopic evolution diagram was modified after Chen and Jahn (1998). Major crustal formation events are represented by the protoliths of the Badu, Hexi-Jian'ou, Longquan-Mayuan Groups. Most Phanerozoic granitoids from the region were probably formed by remelting of ancient Proterozoic crust (Chen and Jahn, 1998). The Shuikoushan granodiorites have negative $\varepsilon_{Nd}(t)$ values, suggesting that middle–lower crustal rocks were involved in their petrogenesis.

the first stage of melting, which progressively advances the dehydration-melting of amphibolite in generating water-unsaturated melts (Wolf and Wyllie, 1994; Rapp and Watson, 1995). A large increase in melts, along with the loss of amphibole and the decrease of plagioclase, occurs when clinopyroxene and garnet increase (Wolf and Wyllie, 1994). Garnet forms from the breakdown of amphibole and plagioclase: plagioclase + amphibole ± quartz = garnet + clinopyroxene + amphibole + plagioclase + melt (Wolf and Wyllie, 1994; Zhao et al., 2007). Thus, the garnet, amphibole, and plagioclase may be major stable residual phase after melt extraction. The dehydration melting of mafic rock requires a temperature greater than 850 °C (Beard and Lofgren,

**Table 3**
Whole-rock Sr–Nd isotopic compositions of the Shuikoushan granodiorites.

| Sample | $^{87}Rb/^{86}Sr$ | $^{87}Sr/^{86}Sr$ | ±2σ | $(^{87}Sr/^{86}Sr)i$ | $^{143}Nd/^{144}Nd$ | ±2σ | $^{147}Sm/^{144}Nd$ | $(^{143}Nd/^{144}Nd)i$ | $\varepsilon_{Nd}(t)$ | $f_{Sm/Nd}$ | $T_{DM}$ (Ga) | $T_{2DM}$ (Ga) |
|---|---|---|---|---|---|---|---|---|---|---|---|---|
| SKS-6 | 0.778 | 0.711854 | 6 | 0.7101 | 0.512231 | 5 | 0.107 | 0.512120 | −6.13 | −0.46 | 1.31 | 1.44 |
| SKS-31 | 0.764 | 0.711820 | 9 | 0.7101 | 0.512255 | 3 | 0.120 | 0.512131 | −5.92 | −0.39 | 1.45 | 1.43 |
| SKS-36 | 0.749 | 0.711845 | 7 | 0.7102 | 0.512241 | 3 | 0.116 | 0.512121 | −6.12 | −0.41 | 1.42 | 1.44 |
| SKS-50 | 0.782 | 0.711864 | 7 | 0.7101 | 0.512248 | 15 | 0.113 | 0.512131 | −5.93 | −0.42 | 1.37 | 1.43 |

Note: $^{87}Rb/^{86}Sr$ and $^{147}Sm/^{144}Nd$ are calculated using whole-rock Rb, Sr, Sm, Nd concentrations determined by ICP-MS. $\varepsilon_{Nd}(t)$ values are calculated using present-day $(^{147}Sm/^{144}Nd)_{CHUR}$ = 0.1967 and $(^{143}Nd/^{144}Nd)_{CHUR}$ = 0.512638 (Goldstein and Jacobsen, 1988). $T_{DM}$ values are calculated using present-day $(^{147}Sm/^{144}Nd)_{DM}$ = 0.2137 and $(^{143}Nd/^{144}Nd)_{DM}$ = 0.51315 (DePaolo, 1981). The single-stage Nd model age ($T_{DM}$) is calculated as same as (Li et al., 2003b); the two-stage Nd model age ($T_{2DM}$) is calculated using the same formulation as (Keto and Jacobsen, 1987). The decay constant $\lambda_{Sm–Nd}$ = 6.54 × $10^{-12}$ per year. Sr–Nd isotopes are corrected at $t$ = 158.3 Ma.

**Table 4**
Zircon Hf–O isotopic data for the Shuikoushan granodiorites.

| Sample and spot | $^{176}Lu/^{177}Hf$ | ±1σ | $^{176}Hf/^{177}Hf$ | ±1σ | $t$ (Ma) | $(^{176}Hf/^{177}Hf)i$ | $\varepsilon_{Hf}(t)$ | ±1σ | $f_{Lu/Hf}$ | $T_{DM}$ (Ga) | ±1σ (Ma) | $T_{2DM}$ (Ga) | ±1σ (Ma) | $\delta^{18}O$ (‰) | ±2σ |
|---|---|---|---|---|---|---|---|---|---|---|---|---|---|---|---|
| *Sample SKS-31* | | | | | | | | | | | | | | | |
| SKS-31@01 | 0.00120 | 0.000015 | 0.282424 | 0.000010 | 159.6 | 0.282420 | −8.9 | 0.3 | −0.96 | 1.18 | 13.54 | 1.77 | 21.27 | 9.17 | 0.30 |
| SKS-31@02 | 0.00172 | 0.000038 | 0.282401 | 0.000010 | 156.4 | 0.282396 | −9.9 | 0.4 | −0.95 | 1.23 | 14.56 | 1.82 | 22.50 | 9.43 | 0.46 |
| SKS-31@03 | 0.00129 | 0.000014 | 0.282405 | 0.000008 | 156.2 | 0.282401 | −9.7 | 0.3 | −0.96 | 1.21 | 11.54 | 1.81 | 18.07 | 9.13 | 0.32 |
| SKS-31@04 | 0.00164 | 0.000030 | 0.282428 | 0.000009 | 155.8 | 0.282423 | −8.9 | 0.3 | −0.95 | 1.19 | 13.21 | 1.77 | 20.48 | 9.34 | 0.28 |
| SKS-31@05 | 0.00145 | 0.000019 | 0.282427 | 0.000009 | 153.8 | 0.282423 | −9.0 | 0.3 | −0.96 | 1.18 | 13.43 | 1.77 | 20.95 | 9.33 | 0.41 |
| SKS-31@06 | 0.00170 | 0.000026 | 0.282422 | 0.000011 | 160.8 | 0.282417 | −9.0 | 0.4 | −0.95 | 1.20 | 16.28 | 1.78 | 25.22 | 9.37 | 0.32 |
| SKS-31@07 | 0.00177 | 0.000020 | 0.282445 | 0.000010 | 158.2 | 0.282440 | −8.3 | 0.4 | −0.95 | 1.17 | 15.00 | 1.73 | 23.22 | 9.31 | 0.32 |
| SKS-31@08 | 0.00105 | 0.000039 | 0.282398 | 0.000011 | 155.7 | 0.282395 | −9.9 | 0.4 | −0.97 | 1.21 | 15.41 | 1.83 | 24.24 | 8.83 | 0.41 |
| SKS-31@09 | 0.00175 | 0.000044 | 0.282417 | 0.000012 | 158.4 | 0.282412 | −9.3 | 0.4 | −0.95 | 1.21 | 16.65 | 1.79 | 25.70 | 8.93 | 0.33 |
| SKS-31@10 | 0.00162 | 0.000016 | 0.282421 | 0.000009 | 159.8 | 0.282416 | −9.1 | 0.3 | −0.95 | 1.20 | 12.14 | 1.78 | 18.86 | 9.24 | 0.34 |
| SKS-31@11 | 0.00130 | 0.000023 | 0.282420 | 0.000009 | 155.0 | 0.282416 | −9.2 | 0.3 | −0.96 | 1.19 | 12.25 | 1.78 | 19.18 | 9.35 | 0.38 |
| SKS-31@12 | 0.00170 | 0.000060 | 0.282434 | 0.000009 | 153.4 | 0.282429 | −8.8 | 0.3 | −0.95 | 1.18 | 12.77 | 1.75 | 19.60 | 9.13 | 0.31 |
| SKS-31@13 | 0.00162 | 0.000027 | 0.282412 | 0.000009 | 162.5 | 0.282407 | −9.3 | 0.3 | −0.95 | 1.21 | 13.18 | 1.80 | 20.45 | 8.85 | 0.37 |
| SKS-31@14 | 0.00193 | 0.000025 | 0.282395 | 0.000009 | 157.9 | 0.282390 | −10.1 | 0.3 | −0.94 | 1.24 | 13.61 | 1.84 | 20.94 | 9.28 | 0.28 |
| SKS-31@15 | 0.00160 | 0.000041 | 0.282426 | 0.000010 | 161.2 | 0.282422 | −8.9 | 0.4 | −0.95 | 1.19 | 14.37 | 1.77 | 22.26 | 9.19 | 0.47 |
| SKS-31@16 | 0.00187 | 0.000112 | 0.282409 | 0.000011 | 161.9 | 0.282403 | −9.5 | 0.3 | −0.94 | 1.22 | 15.86 | 1.81 | 23.82 | 9.06 | 0.37 |
| SKS-31@17 | 0.00140 | 0.000043 | 0.282437 | 0.000010 | 164.6 | 0.282432 | −8.4 | 0.4 | −0.96 | 1.17 | 14.66 | 1.74 | 22.84 | 8.74 | 0.39 |
| SKS-31@18 | 0.00312 | 0.000028 | 0.282527 | 0.000011 | 744.8 | 0.282483 | 6.2 | 0.4 | −0.91 | 1.09 | 15.88 | 1.26 | 23.85 | 9.06 | 0.31 |
| SKS-31@19 | 0.00121 | 0.000031 | 0.282391 | 0.000010 | 154.5 | 0.282387 | −10.2 | 0.3 | −0.96 | 1.23 | 13.71 | 1.85 | 21.48 | 9.22 | 0.36 |
| SKS-31@20 | 0.00201 | 0.000025 | 0.282449 | 0.000009 | 161.1 | 0.282443 | −8.1 | 0.3 | −0.94 | 1.17 | 12.82 | 1.72 | 19.69 | 9.10 | 0.35 |
| SKS-31@21 | 0.00158 | 0.000008 | 0.282438 | 0.000009 | 164.9 | 0.282433 | −8.4 | 0.3 | −0.95 | 1.17 | 13.26 | 1.74 | 20.64 | 9.34 | 0.43 |
| SKS-31@22 | 0.00170 | 0.000033 | 0.282422 | 0.000010 | 157.7 | 0.282417 | −9.1 | 0.3 | −0.95 | 1.20 | 13.44 | 1.78 | 20.79 | 8.92 | 0.44 |
| SKS-31@23 | 0.00175 | 0.000014 | 0.282439 | 0.000010 | 155.2 | 0.282434 | −8.5 | 0.4 | −0.95 | 1.17 | 14.79 | 1.74 | 22.90 | 9.35 | 0.45 |
| SKS-31@24 | 0.00134 | 0.000053 | 0.282401 | 0.000009 | 160.9 | 0.282397 | −9.7 | 0.3 | −0.96 | 1.21 | 13.01 | 1.82 | 20.20 | 9.09 | 0.33 |
| SKS-31@25 | 0.00164 | 0.000019 | 0.282440 | 0.000009 | 158.3 | 0.282436 | −8.4 | 0.3 | −0.95 | 1.17 | 12.69 | 1.74 | 19.70 | 9.40 | 0.42 |
| SKS-31@26 | 0.00150 | 0.000016 | 0.282414 | 0.000010 | 158.3 | 0.282410 | −9.3 | 0.3 | −0.95 | 1.20 | 13.92 | 1.79 | 21.69 | | |
| SKS-31@27 | 0.00156 | 0.000026 | 0.282439 | 0.000010 | 158.3 | 0.282435 | −8.5 | 0.3 | −0.95 | 1.17 | 13.77 | 1.74 | 21.40 | | |
| SKS-31@28 | 0.00155 | 0.000021 | 0.282439 | 0.000011 | 158.3 | 0.282434 | −8.5 | 0.4 | −0.95 | 1.17 | 15.40 | 1.74 | 23.98 | | |
| *Sample SKS-36* | | | | | | | | | | | | | | | |
| SKS-36@01 | 0.00156 | 0.000055 | 0.282418 | 0.000009 | 155.4 | 0.282413 | −9.3 | 0.3 | −0.95 | 1.20 | 12.42 | 1.79 | 19.14 | 9.68 | 0.33 |
| SKS-36@02 | 0.00094 | 0.000007 | 0.282444 | 0.000009 | 161.3 | 0.282441 | −8.2 | 0.3 | −0.97 | 1.14 | 12.96 | 1.72 | 20.51 | 9.60 | 0.27 |
| SKS-36@03 | 0.00113 | 0.000011 | 0.282409 | 0.000011 | 161.0 | 0.282406 | −9.4 | 0.4 | −0.97 | 1.20 | 14.83 | 1.80 | 23.34 | 9.48 | 0.33 |
| SKS-36@04 | 0.00113 | 0.000031 | 0.282376 | 0.000010 | 159.5 | 0.282373 | −10.6 | 0.4 | −0.97 | 1.24 | 14.16 | 1.87 | 22.24 | 9.38 | 0.31 |
| SKS-36@05 | 0.00185 | 0.000034 | 0.282429 | 0.000009 | 157.0 | 0.282424 | −8.9 | 0.3 | −0.94 | 1.19 | 13.23 | 1.76 | 20.38 | 9.43 | 0.43 |
| SKS-36@06 | 0.00153 | 0.000033 | 0.282436 | 0.000009 | 160.1 | 0.282431 | −8.5 | 0.3 | −0.95 | 1.17 | 13.38 | 1.74 | 20.80 | 9.28 | 0.40 |
| SKS-36@07 | 0.00128 | 0.000009 | 0.282422 | 0.000010 | 155.1 | 0.282418 | −9.1 | 0.4 | −0.96 | 1.18 | 14.83 | 1.78 | 23.26 | 8.97 | 0.34 |
| SKS-36@08 | 0.00149 | 0.000027 | 0.282421 | 0.000012 | 158.7 | 0.282417 | −9.1 | 0.4 | −0.96 | 1.19 | 16.54 | 1.78 | 25.78 | 9.46 | 0.55 |
| SKS-36@09 | 0.00160 | 0.000022 | 0.282470 | 0.000013 | 158.9 | 0.282466 | −7.4 | 0.5 | −0.95 | 1.12 | 18.75 | 1.67 | 29.17 | 9.20 | 0.41 |
| SKS-36@10 | 0.00100 | 0.000020 | 0.282452 | 0.000010 | 157.2 | 0.282450 | −8.0 | 0.4 | −0.97 | 1.13 | 14.03 | 1.71 | 22.17 | 9.11 | 0.30 |
| SKS-36@11 | 0.00135 | 0.000013 | 0.282432 | 0.000011 | 159.2 | 0.282428 | −8.7 | 0.4 | −0.96 | 1.17 | 15.45 | 1.75 | 24.19 | 8.89 | 0.39 |
| SKS-36@12 | 0.00148 | 0.000041 | 0.282446 | 0.000009 | 158.2 | 0.282441 | −8.2 | 0.3 | −0.96 | 1.16 | 13.47 | 1.72 | 20.94 | 9.03 | 0.46 |
| SKS-36@13 | 0.00146 | 0.000025 | 0.282450 | 0.000011 | 161.8 | 0.282446 | −8.0 | 0.4 | −0.96 | 1.15 | 15.05 | 1.71 | 23.48 | 8.61 | 0.41 |
| SKS-36@14 | 0.00160 | 0.000026 | 0.282427 | 0.000010 | 164.4 | 0.282422 | −8.8 | 0.4 | −0.95 | 1.19 | 14.52 | 1.76 | 22.55 | 9.07 | 0.37 |
| SKS-36@15 | 0.00156 | 0.000034 | 0.282444 | 0.000011 | 156.6 | 0.282439 | −8.3 | 0.4 | −0.95 | 1.16 | 15.11 | 1.73 | 23.49 | 9.09 | 0.34 |
| SKS-36@16 | 0.00206 | 0.000037 | 0.282422 | 0.000012 | 159.4 | 0.282416 | −9.1 | 0.4 | −0.94 | 1.21 | 16.99 | 1.78 | 26.04 | 9.02 | 0.27 |
| SKS-36@17 | 0.00119 | 0.000064 | 0.282431 | 0.000010 | 156.0 | 0.282427 | −8.8 | 0.4 | −0.96 | 1.17 | 14.17 | 1.76 | 22.06 | 8.98 | 0.32 |
| SKS-36@18 | 0.00158 | 0.000024 | 0.282428 | 0.000010 | 158.7 | 0.282423 | −8.9 | 0.4 | −0.95 | 1.18 | 14.41 | 1.76 | 22.40 | 8.40 | 0.29 |
| SKS-36@19 | 0.00145 | 0.000021 | 0.282430 | 0.000010 | 163.8 | 0.282426 | −8.7 | 0.4 | −0.96 | 1.18 | 14.18 | 1.75 | 22.13 | 8.54 | 0.31 |
| SKS-36@20 | 0.00148 | 0.000024 | 0.282439 | 0.000010 | 158.8 | 0.282434 | −8.5 | 0.3 | −0.96 | 1.17 | 13.72 | 1.74 | 21.38 | 9.02 | 0.38 |
| SKS-36@21 | 0.00130 | 0.000018 | 0.282427 | 0.000009 | 158.8 | 0.282423 | −8.8 | 0.3 | −0.96 | 1.18 | 12.91 | 1.76 | 20.23 | | |

Note: Hf–O isotopic data were obtained on the same position of zircon grains; the initial Hf ratios were calculated at corresponding SIMS zircon $^{206}Pb/^{238}U$ age; $\varepsilon_{Hf}(t)$ values are calculated using present-day $(^{176}Lu/^{177}Hf)_{CHUR}$ = 0.0332 and $(^{176}Hf/^{177}Hf)_{CHUR}$ = 0.282772 (Blichert-Toft et al., 1997). $T_{2DM}$ and $T_{DM}$ values are calculated using present-day $(^{176}Lu/^{177}Hf)_{DM}$ = 0.0384 and $(^{176}Hf/^{177}Hf)_{DM}$ = 0.28325 (Griffin et al., 2000). The decay constant of $^{176}Lu$ is 1.865 × $10^{-11}$ year$^{-1}$ (Scherer et al., 2001). $^{176}Lu/^{177}Hf$ ratio of 0.015 for the averaged continental crust (Griffin et al., 2002).
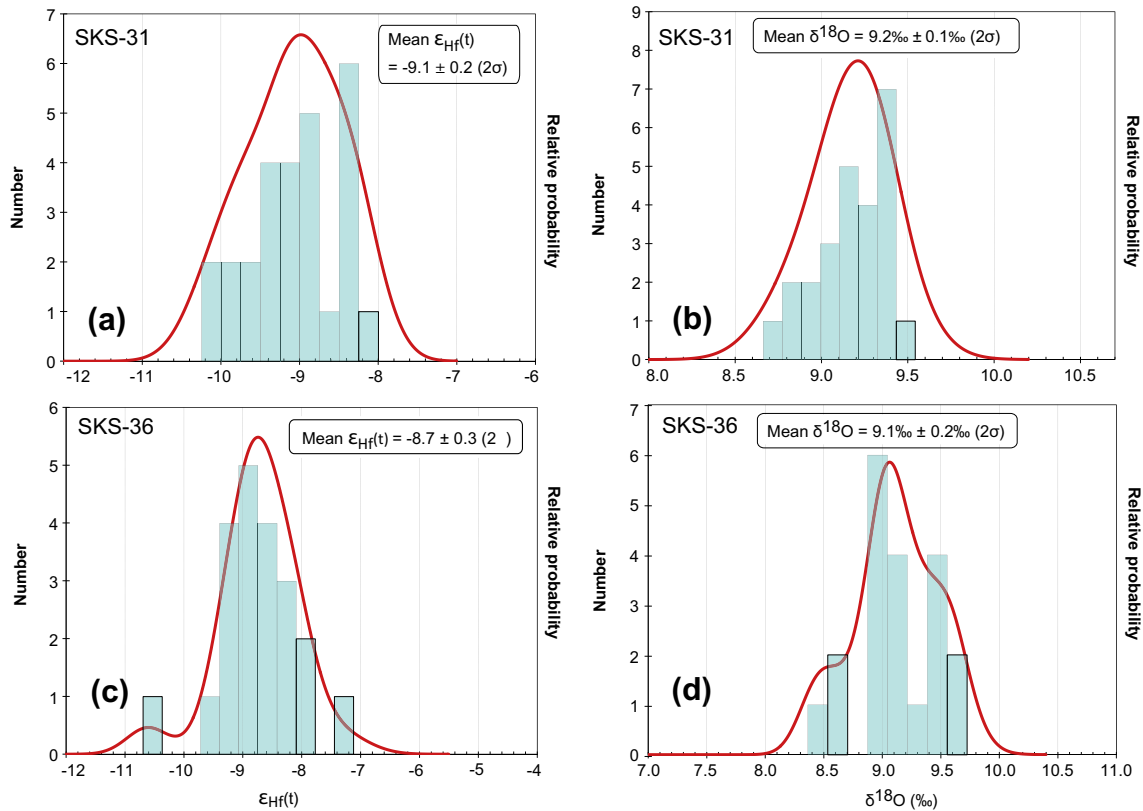
**Fig. 10.** Histogram for zircon $\varepsilon_{Hf}(t)$ and $\delta^{18}O$ values of rocks from the Shuikoushan intrusion.
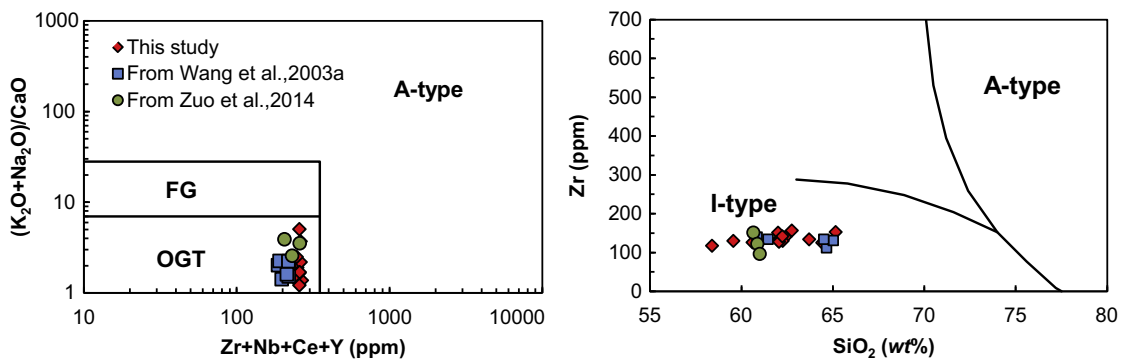


**Fig. 11.** (Na$_2$O + K$_2$O)/CaO vs. Zr + Nb + Ce + Y classification diagram of Whalen et al. (1987). FG = fractionated M-, I-, and S-type granites; OGT = unfractionated M-, I-, and S-type granites. Zr vs. SiO$_2$ classification diagram of Collins et al. (1982).

1991). However, the temperature for lower crustal melting, triggered by underplating, should not be higher than 950 °C (Huppert and Sparks, 1988). At 850–950 °C, the pressure for stability of garnet granulite, as a residual rock containing garnet, amphibole, plagioclase and clinopyroxene, are 1.0–1.5 Gpa in depths of 25–40 km (Drummond et al., 1996; Zhao et al., 2007). Geophysical information suggested that the thickness of crust in southern Hunan Province during Jurassic is less than 40 km (Zhou et al., 2012), which leads us to assume that the crust in this region may probably be middle–lower crust. These estimates have been confirmed by the mafic granulite enclaves in the Jurassic Daoxian basalt at southern Hunan Province, which was conducted under P–T conditions of 0.73 Gpa and 845–950 °C at depths of 25 km (Kong et al., 2000). Thus, we infer that the Shuikoushan peraluminous I-type granitoid samples, as water-unsaturated melt,

may be generated from dehydration-melting of amphibolites in middle–lower crust at relatively high temperature conditions.

### 5.3. Reworking of middle to lower crust beneath Jiangnan orogen

The zircon SIMS U–Pb data of the Shuikoushan granitoids imply magma emplacement at 158 Ma. As previously discussed, it was likely derived from the middle to lower crust. However, it is unclear whether the middle to lower crust is ancient or juvenile. Previous studies suggest that juvenile crust is characterized by a positive $\varepsilon_{Hf}(t)$ value with a young model Hf age, and a low $\delta^{18}O$ value (Zheng et al., 2007). Most of the zircon from Shuikoushan granitoids exhibit a negative $\varepsilon_{Hf}(t)$ value and a high $\delta^{18}O$ value (8.4–9.7‰) with a model Hf age of 1.7–1.9 Ga, thus suggesting a Paleoproterozoic middle–lower crustal origin. The Shuikoushan
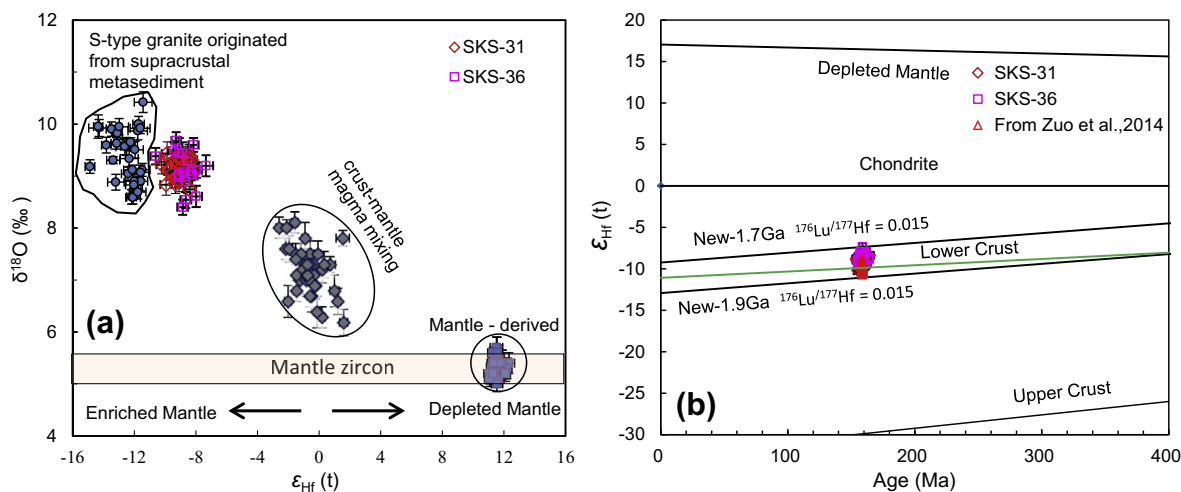
**Fig. 12.** (a) Diagram of Hf vs. O isotopes of zircons from the Shuikoushan and adjacent region intrusive rocks. The Hf–O isotopic compositions of Shuikoushan granodiorites are different from cotemporary mantle-derived (Qinghu granite) and mantle–crust mixing magmas (Lisong granite) in adjacent region (Li et al., 2009a). Compared with tungsten-mineralized supracrust-derived Xihuashan S-type granite (unpublished data), the Shuikoushan granodiorites have relatively high $\varepsilon_{Hf}(t)$ but low $\delta^{18}O$ values. (b) Diagram of Hf isotope evolution in the zircon from the Shuikoushan granodiorites, implying this intrusion formed by "reworking of middle–lower crust" that was primarily extracted from the depleted mantle at ca. 1.7–1.9 Ga. The evolution of depleted mantle at ca. 1.7–1.9 Ga. The evolution of depleted mantle with present-day $^{176}Lu/^{177}Hf = 0.0384$ and $^{176}Hf/^{177}Hf = 0.28325$ (Griffin et al., 2000). Chondrite with present-day $^{176}Lu/^{177}Hf = 0.0332$ and $^{176}Hf/^{177}Hf = 0.282772$, continental upper crust and lower crust with present-day $^{176}Lu/^{177}Hf = 0.0093$ and 0.022, respectively (Wu et al., 2007 and references therein). The corresponding lines of new-crustal generation are calculated by assuming the $^{176}Lu/^{177}Hf$ ratio of 0.015 for the averaged continental crust (Griffin et al., 2002).

granitoid intrusion is located in the southwest of the suture zone in Hunan Province, which was formed by the amalgamation of the Yangtze and the Cathaysia blocks along the Jiangnan orogen at ca. 830 Ma (Zhao et al., 2011; Zhao, 2015). It is unclear whether the Paleoproterozoic middle–lower crustal source for generating Shuikoushan granitoid intrusion is similar to the crust of the Yangtze Block, Cathaysia Block or Jiangnan orogen (Li et al., 2003a; Wang et al., 2003b; Rao et al., 2012). Paleoproterozoic crust has been extrapolated within the Yangtze, Cathaysia, and Jiangnan orogen based on detrital zircon ages and Hf isotopes (Zheng and Zhang, 2007; Wang et al., 2010; Yu et al., 2010; Zhang and Zheng, 2013). However, there is a Neoproterozoic fingerprint in the Shuikoushan granitoids with an inheriting zircon age of 745 Ma (Fig. 4b). The Neoproterozoic rocks (830–740 Ma) are intensively and extensively distributed in Jiangnan orogen, and their Hf model ages are primarily middle Paleoproterozoic (Zhang and Zheng, 2013). The Shuikoushan granitoid magmas may have been contaminated by insignificant Neoproterozoic wall rocks in the Jiannan orogen during emplacement. Additionally, available geochronological data for Mesozoic granitoid rocks and mineralization events statistically in the Jiangnan orogen cluster to 150–160 Ma (Peng et al., 2008), with peaks of 158 Ma (Yang et al., 2012; Wang et al., 2013), coincide with the timing of the Shuikoushan granitoid intrusion. The Sr–Nd isotopic compositions of Shuikoushan intrusion especially coincide with some contemporaneous intrusions from the Jiannan orogen (e.g., the Qitianling intrusion) (Fig. 9a). Thus, we prefer that the Shuikoushan granitoids resulted from the reworking of ancient middle–lower crust beneath the Jiangnan orogen during the late Jurassic period.
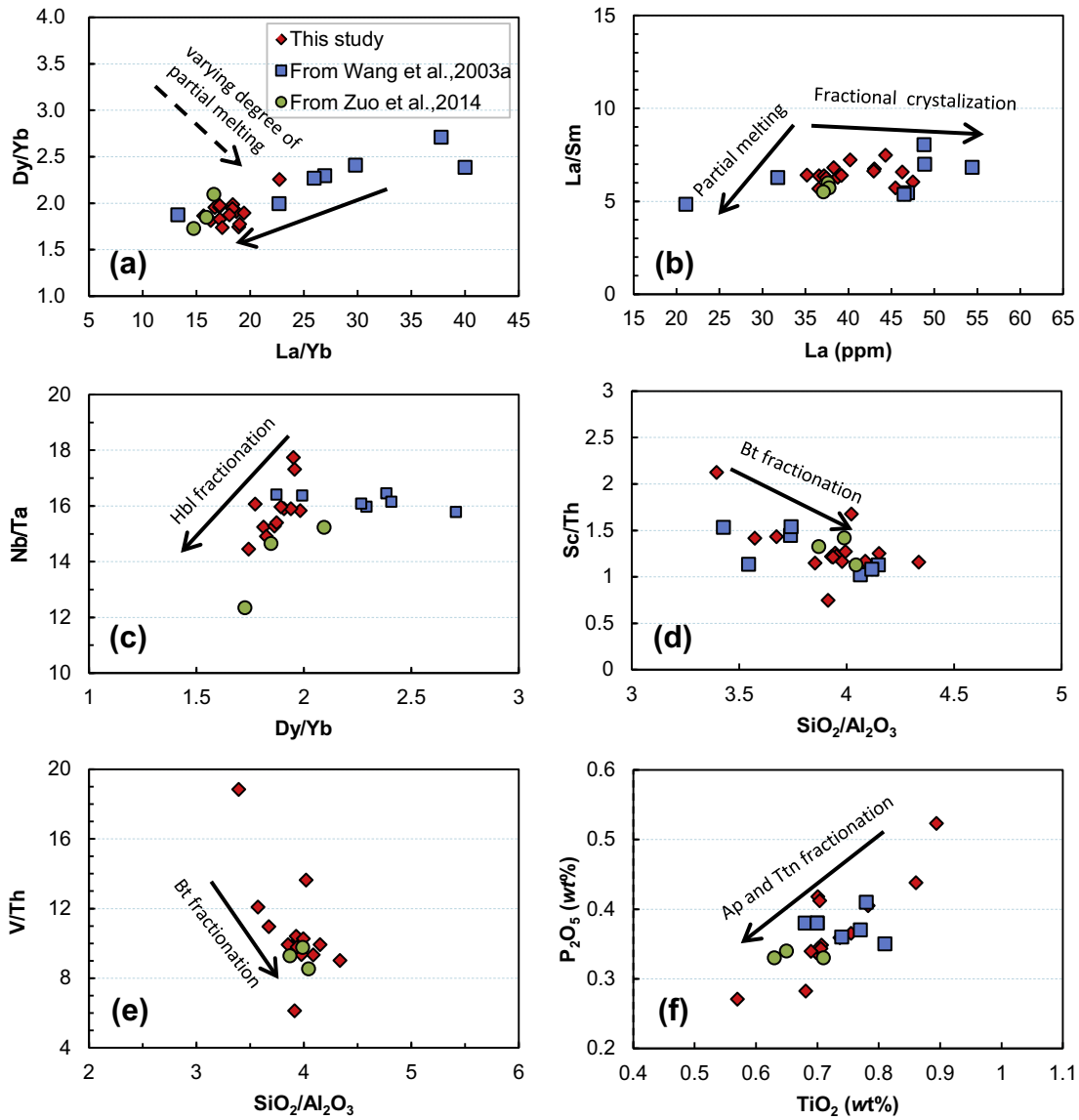
### 5.4. Fractional crystallization

The Shuikoushan granitoids have variable major and trace element compositions. They show negative correlations for $FeO_{(Total)}$, MgO, $TiO_2$, $Al_2O_3$, and $P_2O_5$ against $SiO_2$ (Fig. 6). In addition, Nb–Ta–Ti negative anomalies in the primitive-mantle normalized diagram are present as well (Fig. 8a). A positive correlation between La/Yb and Dy/Yb ratios can also be seen in Fig. 13a. Furthermore, the La/Sm ration remains constant as La concentration

increases (Fig. 13b). Previous studies suggest that these compositional variations may have resulted from fractional crystallization (Allègre and Minster, 1978). The progressive decrease in $FeO_{(Total)}$, MgO, and $Al_2O_3$ as $SiO_2$ content increases indicates the fractionation of mafic minerals. A positive correlation between Nb/Ta and Dy/Yb ratios in the Shuikoushan granitoids strongly suggests amphibole fractionation (Fig. 13c), owing to its $K_D(Nb)/K_D(Ta)$ and $K_D(Dy)/K_D(Yb)$ values exceeding 1.0 (Sisson, 1994; Tiepolo et al., 2001). The fractionation of amphibole can lower the Nb/Ta and Dy/Yb ratios and cause a positive correlation between Nb/Ta and Dy/Yb ratios in the remaining melt. Biotite has an extremely high $K_D$ for Sc and V, but a low value for Th (Bea et al., 1994). Additionally, it contains a high $Al_2O_3$ concentration. Thus, biotite fractionation can increase $SiO_2/Al_2O_3$ but lower Sc/Th and V/Th ratios in residual melts.

Negative correlations between Sc/Th, V/Th, and $SiO_2/Al_2O_3$ ratios in the Shuikoushan granitoids may possibly be related to biotite fractionation (Fig. 13d–e). Moreover, negative anomalies of Nb, Ta, and Ti are considered to be related to the fractionation of the Ti-bearing phase, such as titanite. The progressive decrease in $P_2O_5$ content in granitoid samples may result from apatite fractionation. The REE partition coefficients of these fractionated minerals in intermediate–acid melts increase with atomic number, especially for MREE (Arth, 1976; Bea et al., 1994); and the amphibole and titanite have a weak but positive Eu anomaly (Arth, 1976). This mineral assemblage fractionated from magmas will produce a dramatic depletion in MREE and a concomitant decrease in HREE (Fig. 6i) with an insignificant negative Eu anomaly, which is consistent with the REE pattern of the Shuikoushan granitoids (Fig. 8a). Therefore, varying degrees of hornblende, biotite, titanite, and apatite fractional crystallization may be the main mechanism responsible for the variations in the chemical composition of the Shuikoushan granitoids.

### 5.5. Geodynamic setting for generating Shuikoushan granitoids

South China is characterized by widespread exposed granitoids and intermediate–acid igneous rocks of the Jurassic and Cretaceous age (also named Yangshanian period in Chinese literature) (Fig. 1).

**Fig. 13.** (a) Dy/Yb vs. La/Ya, (b) La/Sm vs. La, (c) Nb/Ta vs. Dy/Yb, (d) Sc/Th vs. SiO$_2$/Al$_2$O$_3$, (e) V/Th vs. SiO$_2$/Al$_2$O$_3$, and (f) P$_2$O$_5$ vs. TiO$_2$ diagrams for the Shuikoushan granodiorites, suggesting mineral fractional crystallization.

Many models were proposed to explain the Mesozoic magmatism in the last few decades (Gilder et al., 1996; Zhou and Li, 2000; Li et al., 2003a; Xie et al., 2006; Wang et al., 2007; Sun et al., 2010). These models can be summarized into two groups, interplate extension/rifting and westward subduction of the paleo-Pacific plate. The westward subduction of the paleo-Pacific plate beneath the Eurasian continental plate is the most popular model for understanding the Yanshanian tectonics in the South China as of the present, although different subduction patterns of the Pacific plate have been proposed (Jahn et al., 1990; Zhou and Li, 2000; Li et al., 2007). However, no geochemical record of the Pacific oceanic crust has been found in late Jurassic igneous rocks from the southern Hunan Province. Some researchers suggested that the Jurassic mantle beneath the southern Hunan Province was homogeneous and undisturbed, and therefore unaffected by the paleo-Pacific subduction system (Chen et al., 2008). Alternatively, it has also been suggested that an extensional tectonic regime in interior of South China may have initiated in the Jurassic (Gilder et al., 1996 and references therein). However, the intraplate extension model

fails to explain what tectonic process and dynamic mechanism drove intraplate extension. Thus, the tectonic regime and geodynamic mechanism in South China during the Mesozoic remain to be disputed and a subject of controversy.

Based on our study, the Shuikoushan granitoids from southern Hunan Province of South China were probably derived from dehydration melting of amphibolite in the middle to lower crust of this region. As aforementioned, dehydration melting of mafic middle to lower crust requires temperatures in excess of ca. 850 °C (Beard and Lofgren, 1991; Zhao et al., 2007). The heating of crustal rocks to such temperatures demands an additional heat supply from the mantle (Patiño-Douce and McCarthy, 1998). Previous studies suggest that the Mesozoic superplume event was of a global scale and related to mantle overturn (Machetel and Humler, 2003). The Pacific superplume event, as an important constituent, may have occurred beneath the Eurasian continent and supplied the excess heat to fuse the lithospheric mantle and overlying crust in the target areas (Zhao et al., 2007). The coeval mafic–ultramafic rocks in the southern Hunan Province serve as evidence that the basaltic
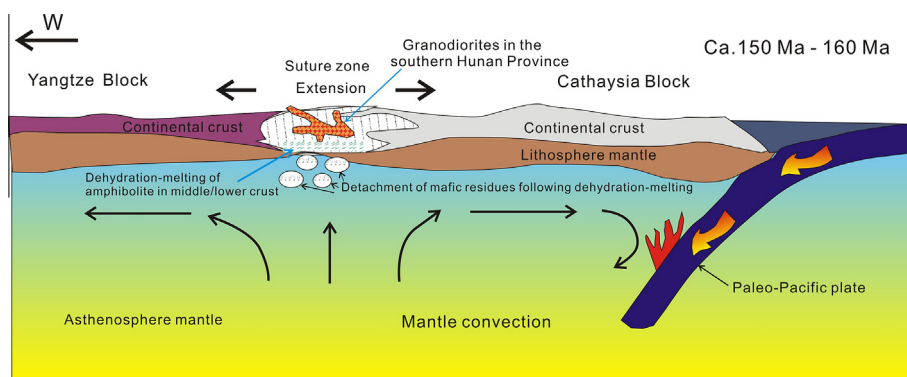
**Fig. 14.** Cartoon illustrating the formation of the Mesozoic granodiorites in the Jiangnan orogen between the Yangtze and the Cathaysia blocks in southern Hunan Province, South China. The late Jurassic Shuikoushan granodiorites were generated by the amphibole-dehydration melting of a mafic source in the middle-to-lower crust due to lithospheric extension.

magma may have acted as a heat source to trigger the dehydration melting of a mafic source in the middle–lower crust.

At the same time, the opening of the south Atlantic and India oceans were drove by the Pacific superplume, which forced the Pacific plate subducted beneath the Eurasian continent (Golonka and Bocharova, 2000). However, the direction of the Pacific plate subduction beneath the Eurasian plate altered from northwest to west between the late Jurassic and early Cretaceous periods, corresponding to the conversion of the tectonic system from EW to NNE trend in South China (Ratschbacher et al., 2000). Regional extension and thinning of the suture zone between the Yangtze and Cathaysia blocks also occurred in this period along the Jiangnan orogen. Accordingly, direction and magnitude of mantle convection beneath the eastern part of the Eurasian continent may have altered as well. As a result, the large-scale magmatism took place between the Jurassic and Cretaceous in South China. The Shuikoushan granitoid intrusion was emplaced during the late Jurassic (158 Ma) and occurred near the Jurassic Shi-Hang rift zone with A-type granitoids of the same age (Fig. 1). This is considered to be formed at an extensional regime (Gilder et al., 1996). Thus, it is reasonable to conclude that the Shuikoushan granitoids were formed from the partial melting of the middle–lower crust due to lithospheric extension, in response to both the Pacific superplume activity and the subduction of the Pacific plate (Fig. 14).

The suture zone is thought to be of arc-continent collision belt between the two blocks (Zhang and Zheng, 2013; Zheng et al., 2013). When the direction of the Pacific plate subduction was converted and the mantle overturned, lithospheric extension susceptibly developed along the ancient orogeny at late Jurassic. Under this condition, the bulging of the asthenospheric mantle may have resulted in remelting and major crustal reworking. The gravitational instability of over-thickened lithospheric mélange of the suture zone favored the detachment that likely occurred in the more ductile parts of the lower crust (Zhao et al., 2007). As previously mentioned, the Shuikoushan granitoids in the southern Hunan Province were generated from dehydration-melting amphibolite at depths of 25–40 km. This is more than the present average crustal depth of ca. 30 km in the southern Hunan Province (Zhou et al., 2012). Thus, it is possible that this crustal thinning was caused by detachment in association with the formation of the granitoids, thus resulting in the detachment of mafic residues. The mafic residues formed after the partial melting at middle/lower crust depths had high densities and were thus susceptible to detachment from the suture zone (Fig. 14). Therefore, the detachment of mafic residues took place after the partial melting of the middle/lower crust, which was triggered by thermal pulse related to the mantle upwelling event.

## 6. Conclusions

New SIMS zircon U–Pb ages confirm that the Shuikoushan granitoid intrusion was emplaced during late Jurassic period with an age of $158.3 \pm 1.2$ Ma. Based on petrography, geochemistry, whole-rock Sr–Nd isotopic, and zircon Hf–O isotopic studies, it can be concluded that the Shuikoushan granitoids are peraluminous I-type granodiorite and were derived from the partial melting of the middle–lower crust beneath Jiangnan orogen. The extensive fractional crystallization of hornblende, biotite, titanite, and apatite may have played an important role in forming the Shuikoushan granitoids with diverse compositions.

The Shuikoushan granitoid intrusion is located in the suture zone between the Yangtze Block and the Cathaysia Block, but was generated from dehydration melting of amphibolites within the Jiangnan orogen. It was produced by the lithospheric extension in response to the subduction of the Pacific plate and the Pacific superplume event. During lithospheric extension, basaltic underplating and asthenospheric upwelling contributed significant heat to trigger partial melting of the middle/lower crust. The detachment of mafic residues took place after the dehydration-melting of amphibolite.

## References

Allègre, C.J., Minster, J.F., 1978. Quantitative models of trace element behavior in magmatic processes. Earth Planet. Sci. Lett. 38, 1–25.

Arth, J.G., 1976. Behavior of trace-elements during magmatic processes – summary of theoretical models and their applications. J. Res. US Geol. Surv. 4, 41–47.

Barbarin, B., 1988. Field evidence for successive mixing and mingling between the Piolard diorite and the Saint-Julien-La-Vetre monzogranite (Nord-Forez, Massif Central, France). Can. J. Earth Sci. 25, 49–59.

Barbarin, B., 1996. Genesis of the two main types of peraluminous granitoids. Geology 24, 295–298.

Bea, F., Pereira, M.D., Stroh, A., 1994. Mineral/leucosome trace-element partitioning in a peraluminous migmatite (a laser ablation-ICP-MS study). Chem. Geol. 117, 291–312.

Beard, J., Lofgren, G., 1991. Dehydration melting and water-saturated melting of basaltic and andesitic greenstones and amphibolites at 1, 3, and 6.9 kb. J. Petrol. 32, 365–401.

Blichert-Toft, J., Chauvel, C., Albarède, F., 1997. Separation of Hf and Lu for high-precision isotope analysis of rock samples by magnetic sector-multiple collector ICP-MS. Contrib. Miner. Petrol. 127, 248–260.

Castro, A., Douce, A.E.P., Corretgé, L.G., Jesús, D., El-Biad, M., El-Hmidi, H., 1999. Origin of peraluminous granites and granodiorites, Iberian massif, Spain: an experimental test of granite petrogenesis. Contrib. Miner. Petrol. 135, 255–276.

Cawthorn, R.G., Brown, P.A., 1976. A model for the formation and crystallization of corundum-normative calc-alkaline magmas through amphibole fractionation. J. Geol., 467–476

Chappell, B., 1999. Aluminium saturation in I- and S-type granites and the characterization of fractionated haplogranites. Lithos 46, 535–551.

Chappell, B., White, A., 1974. Two contrasting granite types. Pac. Geol. 8, 173–174.

Chappell, B., White, A., 1992. I- and S-type granites in the Lachlan Fold Belt. Trans. R. Soc. Edinburgh: Earth Sci. 83, 1–26.

Chappell, B., White, A.J.R., 2001. Two contrasting granite types: 25 years later. Aust. J. Earth Sci. 48, 489–499.

Chappell, B.W., Bryant, C.J., Wyborn, D., 2012. Peraluminous I-type granites. Lithos 153, 142–153.

Chen, C.-H., Lee, C.-Y., Shinjo, R., 2008. Was there Jurassic paleo-Pacific subduction in South China?: Constraints from $^{40}Ar/^{39}Ar$ dating, elemental and Sr–Nd–Pb isotopic geochemistry of the Mesozoic basalts. Lithos 106, 83–92.

Chen, J., Jahn, B.-M., 1998. Crustal evolution of southeastern China: Nd and Sr isotopic evidence. Tectonophysics 284, 101–133.

Chen, J.-F., Foland, K., Xing, F.-M., Xiang, X., Zhou, T.-X., 1991. Magmatism along the southeast margin of the Yangtze block: Precambrian collision of the Yangtze and Cathaysia blocks of China. Geology 19, 815–818.

Chen, Y., Song, S., Niu, Y., Wei, C., 2014. Melting of continental crust during subduction initiation: a case study from the Chaidanuo peraluminous granite in the North Qilian suture zone. Geochim. Cosmochim. Acta 132, 311–336.

Clemens, J.D., Stevens, G., Farina, F., 2011. The enigmatic sources of I-type granites: the peritectic connexion. Lithos 126, 174–181.

Collins, W., Beams, S., White, A., Chappell, B., 1982. Nature and origin of A-type granites with particular reference to southeastern Australia. Contrib. Miner. Petrol. 80, 189–200.

Davis, J., Hawkesworth, C., 1993. The petrogenesis of 30–20 Ma basic and intermediate volcanics from the Mogollon-Datil Volcanic Field, New Mexico, USA. Contrib. Miner. Petrol. 115, 165–183.

DePaolo, D.J., 1981. A neodymium and strontium isotopic study of the Mesozoic calc-alkaline granitic batholiths of the Sierra Nevada and Peninsular Ranges, California. J. Geophys. Res.: Solid Earth 86, 10470–10488.

Douce, A.E.P., 1999. What do experiments tell us about the relative contributions of crust and mantle to the origin of granitic magmas? In: Understanding Granites: Integrating New and Classical Techniques, vol. 168, pp. 55–75.

Drummond, M.S., Defant, M.J., Kepezhinskas, P.K., 1996. Petrogenesis of slab-derived trondhjemite–tonalite–dacite/adakite magmas. Geological Society of America Special Papers, vol. 315, pp. 205–215.

Fisher, C.M., Vervoort, J.D., Hanchar, J.M., 2014. Guidelines for reporting zircon Hf isotopic data by LA-MC-ICPMS and potential pitfalls in the interpretation of these data. Chem. Geol. 363, 125–133.

Gilder, S.A., Gill, J., Coe, R.S., Zhao, X., Liu, Z., Wang, G., Yuan, K., Liu, W., Kuang, G., Wu, H., 1996. Isotopic and paleomagnetic constraints on the Mesozoic tectonic evolution of south China. J. Geophys. Res.: Solid Earth (1978–2012) (101), 16137–16154.

Goldstein, S.J., Jacobsen, S.B., 1988. Nd and Sr isotopic systematics of river water suspended material: implications for crustal evolution. Earth Planet. Sci. Lett. 87, 249–265.

Golonka, J., Bocharova, N.Y., 2000. Hot spot activity and the break-up of Pangea. Palaeogeogr. Palaeoclimatol. Palaeoecol. 161, 49–69.

Griffin, W., Wang, X., Jackson, S., Pearson, N., O'Reilly, S.Y., Xu, X., Zhou, X., 2002. Zircon chemistry and magma mixing, SE China: in-situ analysis of Hf isotopes, Tonglu and Pingtan igneous complexes. Lithos 61, 237–269.

Griffin, W.L., Pearson, N.J., Belousova, E., Jackson, S.E., van Achterbergh, E., O'Reilly, S.Y., Shee, S.R., 2000. The Hf isotope composition of cratonic mantle: LAM-MC-ICPMS analysis of zircon megacrysts in kimberlites. Geochim. Cosmochim. Acta 64, 133–147.

Healy, B., Collins, W.J., Richards, S.W., 2004. A hybrid origin for Lachlan S-type granites: the Murrumbidgee Batholith example. Lithos 78, 197–216.

Hu, Z., Liu, Y., Gao, S., Liu, W., Zhang, W., Tong, X., Lin, L., Zong, K., Li, M., Chen, H., Zhou, L., Yang, L., 2012. Improved in situ Hf isotope ratio analysis of zircon using newly designed X skimmer cone and jet sample cone in combination with the addition of nitrogen by laser ablation multiple collector ICP-MS. J. Anal. At. Spectrom. 27, 1391–1399.

Huang, J.-C., Peng, J.-T., Yang, J.-H., Zhang, B.-L., Xu, C.-X., 2015. Precise zircon U–Pb and molybdenite Re–Os dating of the Shuikoushan granodiorite-related Pb–Zn mineralization, southern Hunan, South China. Ore Geol. Rev. 71, 305–317.

Huppert, H.E., Sparks, R.S.J., 1988. The generation of granitic magmas by intrusion of basalt into continental crust. J. Petrol. 29, 599–624.

Jahn, B.M., Zhou, X.H., Li, J.L., 1990. Formation and tectonic evolution of southeastern China and Taiwan: isotopic and geochemical constraints. Tectonophysics 183, 145–160.

Jahn, B.-M., Cornichet, J., Cong, B., Yui, T.-F., 1996. Ultrahigh-εNd eclogites from an ultrahigh-pressure metamorphic terrane of China. Chem. Geol. 127, 61–79.

Jiao, W., Wu, Y., Yang, S., Peng, M., Wang, J., 2009. The oldest basement rock in the Yangtze Craton revealed by zircon U–Pb age and Hf isotope composition. Sci. China, Ser. D: Earth Sci. 52, 1393–1399.

Jin, Y.-L., Luo, H.-B., 2012. The relationship of the magmatic rocks and ore deposit in Shuikoushan ore field. Land and Resources Herald, pp. 86–88 (in Chinese).

Kemp, A., Hawkesworth, C., Foster, G., Paterson, B., Woodhead, J., Hergt, J., Gray, C., Whitehouse, M., 2007. Magmatic and crustal differentiation history of granitic rocks from Hf–O isotopes in zircon. Science 315, 980–983.

Keto, L.S., Jacobsen, S.B., 1987. Nd and Sr isotopic variations of Early Paleozoic oceans. Earth Planet. Sci. Lett. 84, 27–41.

King, P., White, A., Chappell, B., Allen, C., 1997. Characterization and origin of aluminous A-type granites from the Lachlan Fold Belt, southeastern Australia. J. Petrol. 38, 371–391.

Kong, H., Jin, Z.-M., Lin, Y.-X., 2000. Petrology and chronology of granulite xenolithin Daoxian County, Hunan Province. J. Changchun Univ. Sci. Technol. 30, 115–119 (in Chinese with English abstract).

Lackey, J.S., Valley, J.W., Hinke, H.J., 2006. Deciphering the source and contamination history of peraluminous magmas using $\delta^{18}O$ of accessory minerals: examples from garnet-bearing plutons of the Sierra Nevada batholith. Contrib. Miner. Petrol. 151, 20–44.

Li, S.-T., 2011. Characteristics and genesis of the Yaogangxian tungsten polymetallic deposits in Hunan province. China University of Geosciences (Beijing), pp. 36–84 (in Chinese with English abstract).

Li, H., Watanabe, K., Yonezu, K., 2014. Zircon morphology, geochronology and trace element geochemistry of the granites from the Huangshaping polymetallic deposit, South China: implications for the magmatic evolution and mineralization processes. Ore Geol. Rev. 60, 14–35.

Li, X.-H., Chen, Z., Liu, D., Li, W.-X., 2003a. Jurassic gabbro–granite–syenite suites from southern Jiangxi Province, SE China: age, origin, and tectonic significance. Int. Geol. Rev. 45, 898–921.

Li, X.-H., Li, Z.-X., Ge, W., Zhou, H., Li, W., Liu, Y., Wingate, M.T.D., 2003b. Neoproterozoic granitoids in South China: crustal melting above a mantle plume at ca. 825 Ma? Precambr. Res. 122, 45–83.

Li, X.H., Li, Z.X., Li, W.X., Liu, Y., Yuan, C., Wei, G.J., Qi, C.S., 2007. U–Pb zircon, geochemical and Sr–Nd–Hf isotopic constraints on age and origin of Jurassic I- and A-type granites from central Guangdong, SE China: a major igneous event in response to foundering of a subducted flat-slab? Lithos 96, 186–204.

Li, X.H., Li, W.X., Wang, X.C., Li, Q.L., Liu, Y., Tang, G.Q., 2009a. Role of mantle-derived magma in genesis of early Yanshanian granites in the Nanling Range, South China: in situ zircon Hf–O isotopic constraints. Sci. China, Ser. D: Earth Sci. 52, 1262–1278.

Li, X.H., Liu, Y., Li, Q.L., Guo, C.H., Chamberlain, K.R., 2009b. Precise determination of Phanerozoic zircon Pb/Pb age by multicollector SIMS without external standardization. Geochem. Geophys. Geosyst. 10, Q04010. http://dx.doi.org/10.01029/2009GC002400.

Li, X.-H., Li, W.-X., Li, Q.-L., Wang, X.-C., Liu, Y., Yang, Y.-H., 2010a. Petrogenesis and tectonic significance of the ~850 Ma Gangbian alkaline complex in South China: evidence from in situ zircon U–Pb dating, Hf–O isotopes and whole-rock geochemistry. Lithos 114, 1–15.

Li, X.-H., Long, W.-G., Li, Q.-L., Liu, Y., Zheng, Y.-F., Yang, Y.-H., Chamberlain, K.R., Wan, D.-F., Guo, C.-H., Wang, X.-C., Tao, H., 2010b. Penglai zircon megacrysts: a potential new working reference material for microbeam determination of Hf–O isotopes and U–Pb age. Geostand. Geoanal. Res. 34, 117–134.

Li, X.-H., Long, W.-G., Li, Q.-L., Liu, Y., Zheng, Y.-F., Yang, Y.-H., Chamberlain, K.R., Wan, D.-F., Guo, C.-H., Li, X., Tang, G., Gong, B., Yang, Y., Hou, K., Hu, Z., Li, Q., Liu, Y., Li, W., 2013. Qinghu zircon: a working reference for microbeam analysis of U–Pb age and Hf and O isotopes. Chin. Sci. Bull. 58, 4647–4654.

Liu, Y., Gao, S., Hu, Z., Gao, C., Zong, K., Wang, D., 2010. Continental and oceanic crust recycling-induced melt-peridotite interactions in the trans-North China Orogen: U–Pb dating, Hf isotopes and trace elements in zircons from mantle xenoliths. J. Petrol. 51, 537–571.

Lu, Y.-F., Ma, L.-Y., Qu, W.-J., Mei, Y.-P., Chen, X.-Q., 2006. U–Pb and Re–Os isotope geochronology of Baoshan Cu–Mo polymetallic ore deposit in Hunan province. Acta Petrol. Sin. 22, 2483–2492 (in Chinese with English abstract).

Ludwig, K.R., 2008. User's manual for Isoplot 3.70: a geochronological toolkit for Microsoft Excel. Kenneth R. Ludwig.

Ma, L.-Y., Lu, Y.-F., Me, Y.-P., Chen, X.-Q., 2006. Zircon SHRIMP U–Pb dating of granodiorite from Shuikoushan ore-field, Hunan province and its geological significance. Acta Petrol. Sin. 22, 2475–2482.

Machetel, P., Humler, E., 2003. High mantle temperature during Cretaceous avalanche. Earth Planet. Sci. Lett. 208, 125–133.

Martin, H., 1999. Adakitic magmas: modern analogues of Archaean granitoids. Lithos 46, 411–429.

Middlemost, E.A.K., 1994. Naming materials in the magma/igneous rock system. Earth Sci. Rev. 37, 215–224.

Patiño Douce, A.E., 1995. Experimental generation of hybrid silicic melts by reaction of high-Al basalt with metamorphic rocks. J. Geophys. Res.: Solid Earth 100, 15623–15639.

Patiño Douce, A.E., Johnston, A.D., 1991. Phase equilibria and melt productivity in the pelitic system: implications for the origin of peraluminous granitoids and aluminous granulites. Contrib. Miner. Petrol. 107, 202–218.

Patiño-Douce, A.E., McCarthy, T.C., 1998. Melting of crustal rocks during continental collision and subduction. In: Hacker, B., Liou, J. (Eds.), When Continents Collide: Geodynamics and Geochemistry of Ultrahigh-Pressure Rocks. Springer, Netherlands, pp. 27–55.

Peccerillo, A., Taylor, S.R., 1976. Geochemistry of Eocene calcalkaline volcanic rocks from the Kastamonu area, northern Turkey. Contrib. Miner. Petrol. 58, 63–81.

Peng, J.-T., Hu, R.-Z., Yuan, S.-D., Bi, X.-W., Shen, N.-P., 2008. The time ranges of granitoid emplacement and related nonferrous metallic mineralization in Southern Hunan. Geol. Rev. 54, 617–625 (in Chinese with English abstract).

Qi, L., Hu, J., Gregoire, D.C., 2000. Determination of trace elements in granites by inductively coupled plasma mass spectrometry. Talanta 51, 507–513.

Qiu, L., Yan, D.-P., Tang, S.-L., Wang, Q., Yang, W.-X., Wang, J.-B., Tang, X.-L., 2016. Mesozoic geology of Southwestern China: Indosinian foreland overthrusting and subsequent deformation. J. Asian Earth Sci. 122, 91–105.

Rapp, R.P., Watson, E.B., 1995. Dehydration melting of metabasalt at 8–32 kbar: implications for continental growth and crust–mantle recycling. J. Petrol. 36, 891–931.

Ratschbacher, L., Hacker, B.R., Webb, L.E., McWilliams, M., Ireland, T., Dong, S., Calvert, A., Chateigner, D., Wenk, H.-R., 2000. Exhumation of the ultrahigh-pressure continental crust in east central China: Cretaceous and Cenozoic unroofing and the Tan-Lu fault. J. Geophys. Res.: Solid Earth 105, 13303–13338.

Rao, J.-R., Xiao, H.-Y., Liu, Y.-R., Bai, D.-Y., Deng, Y.-L., 2012. Location of the Yangtze-Cathaysia plate convergence zone in Hunan. Chin. J. Geophys. 55, 484–502 (in Chinese with English abstract).

Roberts, M.P., Clemens, J.D., 1993. Origin of high-potassium, calc-alkaline, I-type granitoids. Geology 21, 825–828.

Schaltegger, U., Corfu, F., 1992. The age and source of late Hercynian magmatism in the central Alps: evidence from precise U–Pb ages and initial Hf isotopes. Contrib. Miner. Petrol. 111, 329–344.

Scherer, E., Munker, C., Mezger, K., 2001. Calibration of the lutetium–hafnium clock. Science 293, 683–687.

Sisson, T.W., 1994. Hornblende-melt trace-element partitioning measured by ion microprobe. Chem. Geol. 117, 331–344.

Sláma, J., Košler, J., Condon, D.J., Crowley, J.L., Gerdes, A., Hanchar, J.M., Horstwood, M. S., Morris, G.A., Nasdala, L., Norberg, N., 2008. Plešovice zircon—a new natural reference material for U–Pb and Hf isotopic microanalysis. Chem. Geol. 249, 1–35.

Stacey, J.t., Kramers, J., 1975. Approximation of terrestrial lead isotope evolution by a two-stage model. Earth Planet. Sci. Lett. 26, 207–221.

Sun, S.-S., McDonough, W.F., 1989. Chemical and isotopic systematics of oceanic basalts: implications for mantle composition and processes. Geological Society, London, Special Publications, vol. 42, pp. 313–345.

Sun, T., 2006. A new map showing the distribution of granites in South China and its explanatory notes. Geol. Bull. China 25, 332–335 (in Chinese with English abstract).

Sun, T., Zhou, X., Chen, P., Li, H., Zhou, H., Wang, Z., Shen, W., 2005. Strongly peraluminous granites of Mesozoic in Eastern Nanling Range, southern China: petrogenesis and implications for tectonics. Sci. China, Ser. D: Earth Sci. 48, 165–174.

Sun, W., Ling, M., Yang, X., Fan, W., Ding, X., Liang, H., 2010. Ridge subduction and porphyry copper–gold mineralization: an overview. Sci. China Earth Sci. 53, 475–484.

Sylvester, P.J., 1998. Post-collisional strongly peraluminous granites. Lithos 45, 29–44.

Tiepolo, M., Bottazzi, P., Foley, S.F., Oberti, R., Vannucci, R., Zanetti, A., 2001. Fractionation of Nb and Ta from Zr and Hf at mantle depths: the role of titanian pargasite and kaersutite. J. Petrol. 42, 221–232.

Turpin, L., Cuney, M., Friedrich, M., Bouchez, J.-L., Aubertin, M., 1990. Meta-igneous origin of Hercynian peraluminous granites in N.W. French Massif Central: implications for crustal history reconstructions. Contrib. Miner. Petrol. 104, 163–172.

Ugidos, J., Recio, C., 1993. Origin of cordierite-bearing granites by assimilation in the Central Iberian Massif (CIM), Spain. Chem. Geol. 103, 27–43.

Valley, J.W., Lackey, J.S., Cavosie, A.J., Clechenko, C.C., Spicuzza, M.J., Basei, M.A.S., Bindeman, I.N., Ferreira, V.P., Sial, A.N., King, E.M., Peck, W.H., Sinha, A.K., Wei, C. S., 2005. 4.4 billion years of crustal maturation: oxygen isotope ratios of magmatic zircon. Contrib. Miner. Petrol. 150, 561–580.

Wang, L.-J., Griffin, W.L., Yu, J.-H., O'Reilly, S.Y., 2010. Precambrian crustal evolution of the Yangtze Block tracked by detrital zircons from Neoproterozoic sedimentary rocks. Precambr. Res. 177, 131–144.

Wang, Q., Wyman, D.A., Xu, J.F., Zhao, Z.H., Jian, P., Zi, F., 2007. Partial melting of thickened or delaminated lower crust in the middle of Eastern China: implications for Cu–Au mineralization. J. Geol. 115, 149–161.

Wang, Q., Xu, J.-F., Jian, P., Bao, Z.-W., Zhao, Z.-H., Li, C.-F., Xiong, X.-L., Ma, J.-L., 2006. Petrogenesis of adakitic porphyries in an extensional tectonic setting, Dexing, South China: implications for the genesis of porphyry copper mineralization. J. Petrol. 47, 119–144.

Wang, Y., Fan, W., Guo, F., 2003a. Geochemistry of early Mesozoic potassium-rich diorites–granodiorites in southeastern Hunan Province, South China: petrogenesis and tectonic implications. Geochem. J. – Jpn. 37, 427–448.

Wang, Y., Fan, W., Guo, F., Peng, T., Li, C., 2003b. Geochemistry of Mesozoic mafic rocks adjacent to the Chenzhou-Linwu fault, South China: implications for the lithospheric boundary between the Yangtze and Cathaysia blocks. Int. Geol. Rev. 45, 263–286.

Wang, Y., Fan, W., Zhang, G., Zhang, Y., 2013. Phanerozoic tectonics of the South China Block: key observations and controversies. Gondwana Res. 23, 1273–1305.

Wang, Y.J., Fan, W.M., Guo, F., Li, H.M., Liang, X.Q., 2002. U–Pb dating of early Mesozoic granodioritic intrusions in southeastern Hunan Province, South China and its petrogenetic implications. Chin. Sci. Bull. 45, 280–288.

Wang, Y.-J., Fan, W.-M., Guo, F., Li, X., 2001. Petrological and geochemical characteristics of mesozoic granodioritic intrusions in Southeast Hunan province, China. Acta Petrol. Sin. 17, 169–175 (in Chinese with English abstract).

Whalen, J.B., 1985. Geochemistry of an island-arc plutonic suite: the Uasilau-Yau Yau intrusive complex, New Britain, P.N.G. J. Petrol. 26, 603–632.

Whalen, J.B., Currie, K.L., Chappell, B.W., 1987. A-type granites: geochemical characteristics, discrimination and petrogenesis. Contrib. Miner. Petrol. 95, 407–419.

White, A., Chappell, B., 1983. Granitoid types and their distribution in the Lachlan Fold Belt, southeastern Australia. Geol. Soc. Am. Mem. 159, 21–34.

Wiedenbeck, M., Alle, P., Corfu, F., Griffin, W., Meier, M., Oberli, F., Quadt, A.v., Roddick, J., Spiegel, W., 1995. Three natural zircon standards for U–Th–Pb, Lu–Hf, trace element and REE analyses. Geostand. Newslett. 19, 1–23.

Wolf, M., Wyllie, P., 1994. Dehydration-melting of amphibolite at 10 kbar: the effects of temperature and time. Contrib. Miner. Petrol. 115, 369–383.

Wu, F.-Y., Li, X.-H., Zheng, Y.-F., Gao, S., 2007. Lu–Hf isotopic systematics and their applications in petrology. Acta Petrol. Sin. 23, 185–220 (in Chinese with English abstract).

Wyllie, P.J., Wolf, M.B., 1993. Amphibolite dehydration-melting: sorting out the solidus. Geological Society, London, Special Publications, vol. 76, pp. 405–416.

Xie, C., Zhu, J., Ding, S., Zhang, Y., Li, Z., 2006. Identification of Hercynian shoshonitic intrusive rocks in central Hainan Island and its geotectonic implications. Chin. Sci. Bull. 51, 2507–2519.

Yan, D.P., Zhou, M.F., Song, H.L., Wang, X.W., Malpas, J., 2003. Origin and tectonic significance of a Mesozoic multi-layer over-thrust system within the Yangtze Block (South China). Tectonophysics 361, 239–254.

Yang, J.H., Peng, J.T., Zhao, J.H., Fu, Y.Z., Yang, C., Hong, Y.L., 2012. Petrogenesis of the Xihuashan Granite in Southern Jiangxi Province, South China: constraints from zircon U–Pb geochronology, geochemistry and Nd isotopes. Acta Geol. Sin. 86, 131–152.

Yao, J., Shu, L., Santosh, M., Li, J., 2015. Neoproterozoic arc-related andesite and orogeny-related unconformity in the eastern Jiangnan orogenic belt: constraints on the assembly of the Yangtze and Cathaysia blocks in South China. Precambr. Res. 262, 84–100.

Yu, J.-H., Xu, X., O'Reilly, S.Y., Griffin, W.L., Zhang, M., 2003. Granulite xenoliths from Cenozoic Basalts in SE China provide geochemical fingerprints to distinguish lower crust terranes from the North and South China tectonic blocks. Lithos 67, 77–102.

Yu, J.-H., O'Reilly, S.Y., Wang, L., Griffin, W.L., Zhou, M.-F., Zhang, M., Shu, L., 2010. Components and episodic growth of Precambrian crust in the Cathaysia Block, South China: evidence from U–Pb ages and Hf isotopes of zircons in Neoproterozoic sediments. Precambr. Res. 181, 97–114.

Yuan, Z.-X., Wu, L.-S., Zhang, Z.-Q., Ye, X.-J., 1991. The Sm–Nd, Rb–Sr isotopic age-dating of Mayuan group in Northern Fujian. Acta Petrol. Mineral. 10, 127–132 (in Chinese with English abstract).

Zen, E., 1986. Aluminum enrichment in silicate melts by fractional crystallization: some mineralogic and petrographic constraints. J. Petrol. 27, 1095–1117.

Zen, E.-A., 1988. Phase relations of peraluminous granitic rocks and their petrogenetic implications. Annu. Rev. Earth Planet. Sci. 16, 21.

Zhang, S.-B., Zheng, Y.-F., 2013. Formation and evolution of Precambrian continental lithosphere in South China. Gondwana Res. 23, 1241–1260.

Zhao, G., 2015. Jiangnan Orogen in South China: developing from divergent double subduction. Gondwana Res. 27, 1173–1180.

Zhao, J.-H., Asimow, P.D., 2014. Neoproterozoic boninite-series rocks in South China: a depleted mantle source modified by sediment-derived melt. Chem. Geol. 388, 98–111.

Zhao, J.-H., Zhou, M.-F., Yan, D.-P., Zheng, J.-P., Li, J.-W., 2011. Reappraisal of the ages of Neoproterozoic strata in South China: no connection with the Grenvillian orogeny. Geology 39, 299–302.

Zhao, J.-H., Zhou, M.-F., Zheng, J.-P., 2013. Constraints from zircon U–Pb ages, O and Hf isotopic compositions on the origin of Neoproterozoic peraluminous granitoids from the Jiangnan Fold Belt, South China. Contrib. Miner. Petrol. 166, 1505–1519.

Zhao, K.-D., Jiang, S.-Y., Yang, S.-Y., Dai, B.-Z., Lu, J.-J., 2012. Mineral chemistry, trace elements and Sr–Nd–Hf isotope geochemistry and petrogenesis of Cailing and Furong granites and mafic enclaves from the Qitianling batholith in the Shi-Hang zone, South China. Gondwana Res. 22, 310–324.

Zhao, Z.-F., Zheng, Y.-F., Wei, C.-S., Wu, Y.-B., 2007. Post-collisional granitoids from the Dabie orogen in China: zircon U–Pb age, element and O isotope evidence for recycling of subducted continental crust. Lithos 93, 248–272.

Zheng, Y.-F., Zhang, S.-B., 2007. The formation and evolution of Precambrian continental crust in South China. Chin. Sci. Bull. 52, 1–10 (in Chinese with English abstract).

Zheng, Y.-F., Zhang, S.-B., Zhao, Z.-F., Wu, Y.-B., Li, X., Li, Z., Wu, F.-Y., 2007. Contrasting zircon Hf and O isotopes in the two episodes of Neoproterozoic granitoids in South China: implications for growth and reworking of continental crust. Lithos 96, 127–150.

Zheng, Y.-F., Xiao, W.-J., Zhao, G., 2013. Introduction to tectonics of China. Gondwana Res. 23, 1189–1206.

Zhou, L., Xie, J., Shen, W., Zheng, Y., Yang, Y., Shi, H., Ritzwoller, M.H., 2012. The structure of the crust and uppermost mantle beneath South China from ambient noise and earthquake tomography. Geophys. J. Int. 189, 1565–1583.

Zhou, X., Li, W., 2000. Origin of Late Mesozoic igneous rocks in Southeastern China: implications for lithosphere subduction and underplating of mafic magmas. Tectonophysics 326, 269–287.

Zhu, J.-C., Zhang, P.-H., Xie, C.-F., Zhang, H., Yang, C., 2006. The Huashan-Guposhan A-type granitoid belt in the Western part of the Nanling Mountains: petrology, geochemistry and genetic interpretations. Acta Geol. Sin. 80, 529–542 (in Chinese with English abstract).

Zhu, J.-C., Chen, J., Wang, R.-C., Lu, J.-J., Xie, L., 2008. Early Yanshanian NE trending Sn/W-bearing A-type granites in the Western-middle part of the Nanling Mts region. Geol. J. China Univ. 14, 474–484 (in Chinese with English abstract).

Zuo, C.-H., Lu, R., Zhao, Z.-X., Xu, Z.-W., Lu, J.-J., Wang, R.-C., Chen, J.-Q., 2014. Characterization of element geochemistry, LA-ICP-MS zircon U–Pb age, and Hf isotope of granodiorite in the Shuikoushan deposit, Changning, Hunan Province. Geol. Rev. 60, 811–823 (in Chinese with English abstract).